BIOGENIC SYNTHESIS OF MAGNETITE (Fe_3O_4) NANOPARTICLES USING LEAF EXTRACT OF *Thymus schimperi* AND APPLICATION FOR REMOVAL OF CHROMIUM AND MERCURY IONS FROM AQUEOUS SOLUTION

By: SINTAYEHU TAMMANE GENETI

A THESIS SUBMITTED TO THE DEPARTMENT OF CHEMISTRY

SCHOOL OF APPLIED NATURAL SCIENCE

PRESENTED IN PARTIAL FULFILMENT OF THE REQUIREMENTS

FOR THE DEGREE OF MASTER OF SCIENCE IN CHEMISTRY

OFFICE OF GRADUATE STUDIES

ADAMA SCIENCE AND TECHNOLOGY UNIVERSITY

SEPTEMBER, 2018

ADAMA, ETHIOPIA

BIOGENIC SYNTHESIS OF MAGNETITE (Fe_3O_4) NANOPARTICLES USING LEAF EXTRACT OF *Thymus schimperi* AND APPLICATION FOR REMOVAL OF CHROMIUMANDMERCURY IONS FROM AQUEOUS SOLUTION

BY: SINTAYEHU TAMMANE GENETI

ADVISOR: FEDLU KEDIR (PhD)

CO - ADVISOR: BEDASA ABDISA (PhD)

A THESIS SUBMITTED TO THE DEPARTMENT OF CHEMISTRY SCHOOL OF APPLIED NATURAL SCIENCE

PRESENTED IN PARTIAL FULFILMENT OF THE REQUIREMENTS FOR THE DEGREE OF MASTER OF SCIENCE IN CHEMISTRY

OFFICE OF GRADUATE STUDIES
ADAMA SCIENCE AND TECHNOLOGY UNIVERSITY

SEPTEMBER, 2018
ADAMA, ETHIOPIA

APPROVAL BOARD OF EXAMINERS

We, the undersigned, members of the Board of Examiners of the final open defense by Sintayehu Tammane have read and evaluated his thesis entitled "**BIOGENIC SYNTHESIS OF MAGNETITE (Fe_3O_4) NANOPARTICLES USING LEAF EXTRACT OF *Thymus schimperi* AND APPLICATION FOR REMOVAL OF CHROMIUM AND MERCURY IONS FROM AQUEOUS SOLUTION**" and examined the candidate. This is, therefore, to certify that the thesis has been accepted in partial fulfillment of the requirements of the Degree of Masters of science in Chemistry.

_____	_____	_____
Major Advisor	Signature	Date
_____	_____	_____
Co – advisor	Signature	Date
_____	_____	_____
Chairperson	Signature	Date
_____	_____	_____
Internal Examiner	Signature	Date
_____	_____	_____
External Examiner	Signature	Date

DECLARATION

I hereby declare that this M.Sc Thesis is my original work and has not been presented for a degree in any other university, and all sources of material used for this thesis have been duly acknowledged.

Name: Sintayehu Tammane Geneti Signature:_____

This M.Sc Thesis has been submitted for examination with our approval as thesis advisors.

Advisor: Fedlu Kedir (PhD) Signature:_____

Co-advisor: Bedasa Abdisa (PhD) Signature:_____

Date of submission:_____

ADVISOR'S APPROVAL SHEET

To: Chemistry Department

Subject: Thesis Submission

This is to certify that the thesis entitled "**BIOGENIC SYNTHESIS OF MAGNETITE (Fe_3O_4) NANOPARTICLES USING LEAF EXTRACT OF *Thymus schimperi* AND APPLICATION FOR REMOVAL OF CHROMIUM AND MERCURY IONS FROM AQUEOUS SOLUTION**" submitted in partial fulfillment of the requirements for the degree of Master of Science in Chemistry, the Graduate program of the department of Chemistry, and has been carried out by Sintayehu Tammane ID. No GSU/0504/06, under our supervision. Therefore, we recommend that the student has fulfilled the requirements and hence hereby he can submit the thesis to the department.

_____	_____	_____
Advisor	Signature	Date
_____	_____	_____
Co-Advisor	Signature	Date

DEDICATION

This thesis manuscript is dedicated to my beloved wife Dinke Deressa, my brother Melkamu Tammane and my sons Moibone and Nimona for their concern, love, patience and affection.

ACKNOWLEDGEMENTS

First of all I would like to thank almighty God who gave me strength and wisdom to complete my work successfully.

Then I would like to express my heartfelt gratitude to my advisor, Dr. Fedlu Kedir for his unreserved advice, invaluable suggestion, comments, corrections, professional & technical guidance and friendly approach throughout my work for the successful accomplishment of this thesis.

I would like to express my deepest gratitude to my Co-adviser Dr. Bedasa Abdisa, for his patience, fruitful advice and friendly approach throughout my work.

I would like to express my thanks to Adama Science and Technology University, the Program of Applied Chemistry, and the Program of Applied Biology for providing the necessary knowledge, assistance and facilities to conduct my research work.

Finally, my strongly indebted thanks also extended to my wife W/ro Dinke Deressa and My two sons Moibone and Nimona for thei radvice, patience and all my family members who gave me moral and material support during my study.

TABLE OF CONTENTS

Contents **Pages**

LIST OF FIGURES

Figures **Pages**

LIST OF TABLES

Tables **Pages**

LIST OF APPENDICES

Appendix **Pages**

LIST OF ABBREVIATIONS

Å	Angstron
BET	Brunauer-Emmett-Teller
CB	Conduction Band
Ce	Concentration at Equilibrium
C_o	Initial Concentration
DPC	Diphenylcarbazide
DSSCs	Dye Sensitized Solar Cells
DTA	Differential Thermal Analysis
EDS	Electron Diffraction Spectroscopy
eV	Electron Volt
Fcc	Face center cube
FTIR	Fourier Transformer Infrared
FWHM	Full Width at Half Maximum
HGMS	High Gradient Magnetic Separation
IONPs	Iron Oxide Nanoparticles
kHz	KiloHertz
MNPs	Metal Nanoparticles
MRI	Magnetic Resonance Imaging
NPs	Nanoparticles
PTFE	Polytetrafluoroethylene
Rpm	Revolution Per Minute
SEM	Scanning Electron Microscopy
SMNPs	Spherical Magnetic Nanoparticles
TEM	Transmission Electron Microscopy
UV-Vis	Ultra Violet Visible
VB	Valence Band
XRD	X-Ray Diffraction

ABSTRACT

The progress of green chemistry in the synthesis of nanoparticles using plants has attracted a great attention due to its low cost and non-toxic and environment-friendly nature. The present study focuses on the biogenic synthesis of magnetite (Fe_3O_4) nanoparticles from ferric and ferrous chloride precursor using Thymus schimperi leaf extract and its application for removal of Cr(VI) and Hg(II) ions from aqueous solutions. The synthesized nanoparticles were characterized by advanced techniques like Thermo gravimetric analysis (TGA) which was performed to study the thermal stability showing the results were stable above 450^0C; X-ray diffraction (XRD) spectroscopy revealing desired phase formation and crystal structure having pure cubic face centered phase with particle size in the range of 20-30nm; Fourier Transform Infrared Spectroscopy (FT-IR) which has been used to study the interaction between the capping agents and the synthesized Fe_3O_4 nanoparticles; SEM-EDX analysis revealed information about the sample including external morphology, chemical composition and crystalline structure and orientation of materials making up the sample and UV-Vis characterization technique provided information about the optical properties and band gap energy of the synthesized NPs. *Various factors affecting the removal efficiency such as metal ions initial concentrations, pH, contact time and adsorbent dosage were also studied. The adsorption kinetics followed the Langmuir and Freundlich isotherm models were found to be the predominant for both Cr(VI) and Hg(II) ions removal.*

Keywords: Fe_3O_4 NPs; Biogenic synthesis; *Thymus schimperi*; Adsorption; Chromium removal; Mercury removal.

1. INTRODUCTION

1.1 Background of the study

Nanoscience and nanotechnology are the emerging fields of science which offer a significant scientific and technological advancement in different fields such as medical, electrical, environmental engineering, etc. The word 'nano' comes from the Greek word 'nanos' meaning 'dwarf'. Nano term refers to something of a scale of 10^{-9} m. Nanoscience deals with the study of atoms, molecules, and objects having size on the nanometer scale (Saif *et al*., 2016).

Nanotechnology is the manipulation of matter for the use in particular applications through certain chemical and / or physical processes to create materials having nanosized dimensions in the range of 1-100 nm with the specific properties. Nanoscience is gaining much importance nowadays as the properties such as quantum, mechanical and thermodynamics, which are not visible on the macroscale, are accessible on nanometer scale. New materials with amazing characteristics can be produced by putting molecules with desired properties together. Nanoparticles have greater surface area to volume ratios than larger particles. This causes them to be more reactive and interactive than other materials. Nanoparticles have vast applications in the field of biomedical, electrical, environmental engineering fields, etc (Gangadhara *et al*., 2012; Saif *et al*., 2016; Aerosp *et al*., 2015).

Although nanoparticles can be made using various physicochemical methods, their synthesis using nontoxic and environmentally benign biological methods is attractive especially if they are intended for invasive applications in medicine. Biogenic synthesis is useful not only because of its reduced environmental impact compared with some of the physicochemical production methods, but also because of it can be used to produce large quantities of nanoparticles that are free of contamination and have a well-defined size and morphology. Biosynthesis method is a green chemical and eco-friendly route, and the obtained products exhibit a good biocompatibility (Scheffel *et al*., 2006).

Currently, a large number of physical, chemical, green or biological, and hybrid methods are available to synthesize different types of nanoparticles. The nanoparticles formed by using each method shows specific properties. However, biosynthesis of metal nanoparticles by plants is currently under development. The synthesis of metal nanoparticles using inactivated plant tissue, plant extracts, exudates, and other parts of living plants is a modern alternative for their production. Green synthesis of nanoparticles makes use of environmental friendly, non-toxic and safe reagents (Padil *et al*., 2013).

Green synthesis of metal nanoparticles extracted from different parts (mostly leaf) of the plant is the most effective process of synthesis at a very affordable cost. During the synthesis bioreduction of metal ions takes place (Kanaga *et al*., 2017). Biological systems such as plants, microorganisms produce inorganic materials and most of these are present in nanoscale dimensions (Raveendran *et al*., 2003).

Green nanotechnology has attracted a lot of attention and includes a wide range of processes that reduce or eliminate toxic substances to restore the environment. Plant extract mediated synthesis is an increasing focus of attention. Processes for making nanoparticles using plant extracts are readily scalable, simpler and may be less expensive compared with the relatively expensive methods based on microbial processes and whole plants (Mittal *et al*., 2013).

Thymus schimperi: is indigenous and commonly known as *Tosign* which belongs to *Lamiaceae* family. The leaves are opposite, grayish-green, entire, linear or elliptic, up to 15 mm long. The flowers are small, pale-purple or white, arranged in terminal inflorescences that may be dense or loose. Flowers appear since the beginning of summer until the end of autumn. *Thymus schimperi* is growing on edges of roads, in open grassland, on bare rocks and on slopes, between 2200-4000mm altitudes (Demsew *et al*., 1993).

The major constituents of *Thymus schimperi* are thymol, *p*-cymene, *γ*-terminene and carvacrol. It possesses the essential oils from different species indicating the presence of different components and exhibited strong anti oxidant which could be used as reducing agent to react with ferric ions and as scaffolds to direct the formation of Fe_3O_4 nanoparticles in solution (NigistAsfaw *et al.,* 2000).

Metal oxide nanoparticles have important applications such as magnetic storage media, solar energy transformation, electronics, catalysis and biological applications like imaging, and delivery. Iron oxides are used extensively due to the development of preparation technology of nanometer powders. Magnetite (Fe_3O_4) is a common magnetic iron oxide that has a cubic inverse spinel structure with oxygen forming fcc closed packing and Fe cations occupying interstitial tetrahedral sites and octahedral sites (Senthil *et al*., 2012).

Iron oxide (Fe_3O_4) nanoparticles have attracted intensive research interest because of their important applications in cancer therapy, drug delivery, magnetic resonance imaging (MRI) and wastewater treatment (Vicky *et al*., 2010).

Mercury (II) and chromium (VI) are two toxic and potential carcinogenic metal ions found in various industrial wastewaters, which originate from electroplating, mining activities, battery manufacture, tanneries, paint manufacture, etc. They can accumulate in living organisms and cause various disorders and diseases (Wan Ngah *et al*., 2008).

The main techniques used to remove metal ions from wastewaters are chemical precipitation, ion exchange, membrane filtration, electrolytic methods, reverse osmosis, and adsorption. Among the methods mentioned above, adsorption is an efficient and economical one because of its low initial cost, simplicity of design and easiness of operation (Qin *et al*., 2011).

The main concern of this study was biogenic synthesis of magnetite (Fe_3O_4) nanoparticles by one pot reaction using leaf extracts of *Thymus schimperi,* characterization of nanoparticles using Thermo gravimetric analysis (TGA), X-ray diffraction (X-RD), Fourier transform infrared (FT-IR), Scanning electron microscope (SEM), Electron diffraction spectroscopy (EDS) and Ultra violet visible spectroscopy (UV-Vis) analysis and sorption properties of the prepared magnetite (Fe_3O_4) nanoparticles for mercury and chromium ions removal. A series of batch experiments was conducted to investigate the adsorption of Hg(II) and Cr(VI) ions with the synthesized Fe_3O_4 nanoparticles as the sorbent as well as the influence of pH, contact time and initial concentration of aqueous solutions. The adsorption kinetics and isotherms models were investigated for the possible mechanism.

1.2 Statement of the Problem

Mercury (II) and chromium (VI) are one of the top ten toxic metal ions, are mainly present in the wastewater effluents of various process industries such as paper, pulp and paint, oil refining, rubber processing, and fertilizer plants (Johari *et al*., 2016).

Various conventional treatments to remove heavy metals from aqueous solution include precipitation, electrolysis, ion exchange, cementation, liquid membranes, and liquid-liquid extraction (Crist *et al*., 1996).

However, these processes are ineffective at low metal concentration or expensive due to toxic sludge disposal, chemical reagents for metal recovery, and sorbent regeneration and high energy requirements. Therefore, more effective low cost alternatives are urgently required.

Adsorption technique is an efficient and economical one because of its low initial cost, simplicity of design and easiness of operation (Ilankoon *et al*., 2014). The adsorbents commonly recommended for the removal of heavy metals range from industrial wastes to agricultural waste products, biomaterials and activated carbon (Mohan *et al*., 2006; Gupta *et al*., 2004).

To the best of my knowledge, the use of *Thymus schimperi* leaf extract for biogenic synthesis of Fe_3O_4 NPs and the efficiency of Fe_3O_4 NPs synthesized using *Thymus schimperi* leaf extract for removal of toxic heavy metals such as Cr(VI) and Hg(II) ions from aqueous solutions by adsorption technique has not been reported. So this study was planned to investigate biogenic synthesis of Fe_3O_4 NPs using *Thymus schimperi* leaf extract and to examine its efficiency for removal of chromium and mercury from aqueous solutions.

1.3 Objectives of the Study

1.3.1 General Objective

The study was intended on the biogenic synthesis of Fe_3O_4 NPs using *Thymus schimperi* plant extract and to investigate its efficiency for removal of Cr(VI) and mercury Hg(II) ions from aqueous solutions.

1.3.2 Specific Objectives

The specific objectives of this study were:

i. To synthesize Fe_3O_4 NPs through biological method using *Thymus schimperi* leaf extracts as reducing and capping agent.

ii. To characterize the synthesized Fe_3O_4 NPs using TGA, XRD, FT-IR, SEM, EDS and UV-Vis spectroscopic techniques.

iii. To examine removal efficiency by adsorption of heavy metals; Cr(VI) and Hg(II) ions from aqueous solutions using the synthesized Fe_3O_4 NPs as adsorbent.

1.4 Significance of the study

Fe_3O_4 NPs have promising advantages that can combat environmental pollution. The interest in nanoscale Fe_3O_4 NPs in environmental remediation is increasing due to the reactivity of nanoscale iron having a large surface area to volume ratio (Lin *et al*., 2008; Gui *et al*., 2012).

This study highlights the significance of biogenic synthesis approaches and the role of biocompatible green materials in technological and economically feasible process and practices of *Thymus schimperi*. It also summarizes the quest for an environmental sustainable synthesis process of Fe_3O_4 NPs using *Thymus schimperi* for their application to the field of environmental sustainability like removal of heavy metal ions from aqueous solutions. From the outcome of this study, all communities, scientific communities, industry, new coming researcher will be benefited. This research opens up door for further researches on the use of *Thymus schimperi* in the area.

1.5 Scope of the Study

The scope of this study is limited to synthesis of Fe_3O_4 NPs using *Thymus schimperi;* characterization of the synthesized nanoparticles using TGA, XRD, FTIR, SEM, EDS and UV; and application of the synthesized Fe_3O_4 NPs were exhibited only for removal of heavy metals such as Cr(VI) and Hg(II) ions from aqueous solution.

2. LITERATURE REVIEW

2.1 Nanotechnology and Nanoparticles

Nanotechnology is enabling technology that deals with nano-meter sized objects. It is expected that nanotechnology will be developed at several levels: materials, devices and systems (Feynman *et al*; 1991).

Nanotechnology is the science of materials and devices whose structures and constituents demonstrate novel and considerably altered physical, chemical and biological phenomenon due to their nanoscale size. Thus nanotechnology is defined as the manipulation of matter on an atomic, molecular and super molecular scale involving the design, production, characterization and application of different nanoscale materials in different potential areas providing novel technological advances mainly in the field of medicine (Martin *et al*., 2006).

A nanoparticle can be defined as a microscopic particle that has at least one dimension less than 100 nanometers in size (Thakkar *et al*., 2010). Unlike bulk materials, they have unique optical, thermal, electrical, chemical, and physical properties and, hence, they find a variety of applications in the areas of medicine, chemistry, environment, energy, agriculture, information, and communication, heavy industry, and consumer goods (Panigrahi *et al*., 2004).

The nanoparticles level is the most advanced at present, both in scientific knowledge and in commercial applications. A decade ago, nanoparticles were studied because of their size dependent physical and chemical properties (Murray *et al*., 2000). Now they have entered a commercial exploration period (Paull *et al*., 2003). Nanosize materials have accepted significant attention due to their outstanding physicochemical properties.

Nanoparticles, because of their small size, have distinct properties compared to the bulk form of the same material, thus offering many new developments in the fields of biosensors, biomedicine and bionanotechnology (Madhu *et al.*, 2017).

2.2 Iron oxide nanoparticles

Iron oxide is a mineral compound which occurs abundantly in nature. It presents more than one crystal structure and also different structural and magnetic properties (Machala *et al*., 2011). Eight iron oxides are known (Cornell *et al*., 2003); among these iron oxides, hematite (α-Fe_2O_3), magnetite (Fe_3O_4) and *maghemite* (γ-Fe_2O_3) are very promising and popular candidates due to their polymorphism involving temperature-induced phase transition. Each of these three iron oxides has unique biochemical, magnetic, catalytic, and other properties which provide suitability for specific technical and biomedical applications.

2.2.1 Hematite (α-Fe_2O_3)

As the most stable iron oxide and *n*-type semiconductor under ambient conditions, *hematite*(α-Fe_2O_3) is widely used in catalysts, pigments and gas sensors due to its low cost and high resistance to corrosion. It can also be used as a starting material for the synthesis of magnetite(Fe_3O_4) and *maghemite* (γ-Fe_2O_3), which have been intensively pursued for both fundamental scientific interests and technological applications in the last few decades (Wu *et al*., 2010). Hematite is an *n*-type semiconductor with a band gap of 2.3 eV, where the conduction band (CB) is composed ofempty *d*-orbitals of Fe^{3+} and the valence band (VB) consists of occupied *3d* crystal field orbitals of Fe^{3+} with some admixture from the O 2*p* non-bonding orbitals (Zhang *et al*., 1993). As shown in Figure 1(a), Fe^{3+} ions occupy two-thirds of the octahedral sites that are confined by the nearly ideal hexagonal close-packed O lattice.

2.2.2 Magnetite (Fe_3O_4)

As shown in Figure 1(b), Fe_3O_4 has the face centered cubic spinel structure, based on 32 O^{2-} ions and close-packed along the [111] direction. Fe_3O_4 differs from most other iron oxides in that it contains both divalent and trivalent iron. Fe_3O_4 has a cubic inverse spinel structure that consists of a cubic close packed array of oxide ions, where all of the Fe^{2+} ions occupy half of the octahedral sites and the Fe^{3+} are split evenly across the remaining octahedral sites and the tetrahedral sites. In stoichiometric magnetite Fe^{II}/Fe^{III}= 1/2, and the divalent irons may be partly or fullyreplaced by other divalent ions (Co, Mn, Zn, etc). Thus, Fe_3O_4 can be both an *n*- and *p*-type semiconductor. However, Fe_3O_4 has the lowest resistivity among iron oxides due to its small bandgap (1.0eV) (Boxall *et al*., 1996).

2.2.3 Maghemite (γ-Fe_2O_3)

As shown in Figure 1(c), the structure of γ-Fe_2O_3 is cubic; each unit of *maghemite* contains32 O^{2-} ions, 21⅓ Fe^{3+} ions and 2⅓ vacancies. Oxygen anions give rise to a cubic close-packed array while ferric ions are distributed over tetrahedral sites (eight Fe ions per unit cell) and octahedral sites (the remaining Fe ions and vacancies).Therefore, the *maghemite* can be considered as fully oxidized magnetite, and it is an *n*-type semiconductor with a band gap of 2.0 eV (Jiang *et al*.,2015).

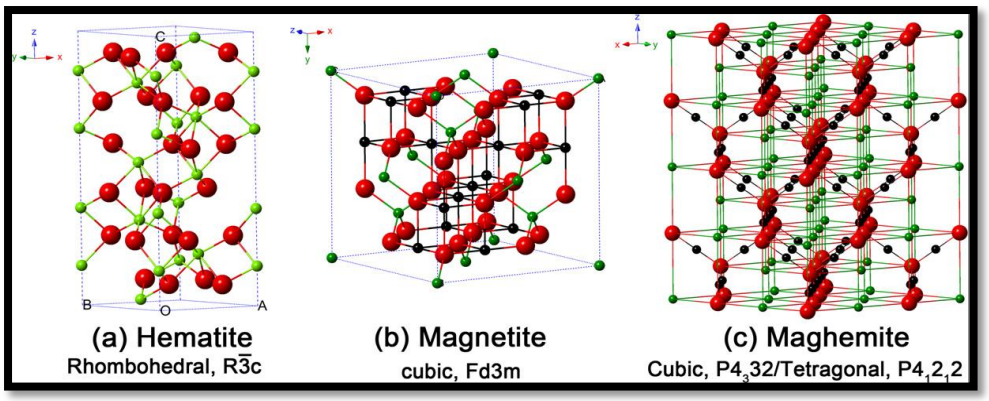

Figure 1: Crystal structure and crystallographic data of (a) hematite, (b) magnetite and (c) maghemite (the black ball is Fe^{2+}, the green ball is Fe^{3+} and the red ball is O^{2-}; Jiang *et al*., 2015).

2.3 Size, shape and magnetic properties of iron oxide nanoparticles

Understanding the correlation between the magnetic properties and the size and shape of IONPs is a prerequisite for widespread applications of magnetism in data storage and bio-separation areas (Xiao *et al*., 2010). Generally, α-Fe_2O_3 has weak ferromagnetism at room temperature, while the saturation magnetization is often smaller than 1 emu g^{-1}. However, γ-Fe_2O_3 and Fe_3O_4 exhibit ferrimagnetism at room temperature, with the saturation magnetization reaching to 92 emu g^{-1}(Yamaura *et al*., 2004). It is noteworthy that many properties of IONPs depend on their size and shape.

Magnetic iron oxides have served humans for centuries, for example, the application of small iron oxide nanoparticles (IONPs) as a contrast agent for *in vitro* diagnostics has been practiced for nearly half a century (Cao *et al*., 2012). Magnetic IONPs are inexpensive to produce, physically and chemically stable, biocompatible, and environmentally safe (Lu *et al*., 2007). Recently, the use of nanosized magnetic nanomaterials as adsorbents has attracted increasing interest due to their high surface area and unique superparamagnetism. These properties lead to high adsorption efficiency, high removal rate of contaminants and easy and rapid separation of adsorbent from solution using magnetic field (Naik *et al*., 2002).

2.4 Synthesis of magnetite Nanoparticles

There are several methods to synthesize magnetite nanoparticles. To date, various popular methods comprising co-precipitation, microemulsion, thermal decomposition, solvothermal, sonochemical, microwave-assisted, chemical vapor deposition, combustion, carbon arc, and laser pyrolysis, have been reported for the preparation of magnetite nanoparticles (Akbarzadeh *et al*., 2012).

In addition, these nanoparticles can also be synthesized by other methods such as electrochemical synthesis (Cabrera *et al*., 2008), laser pyrolysis techniques (Bomati-Miguel *et al*., 2008), microorganism or bacterial synthesis (especially the magnetotactic bacteria and iron reducing bacteria) (Bharde *et al*., 2008), etc. Several novel and effective methods have been developed to synthesize Fe_3O_4 nanomaterials with different shapes, such as nanorods, nanotubes, and hierarchical superstructures (Abbasi *et al*., 2014).

Biological methods of nanoparticle preparation using microorganisms (Abbasi*et al*., 2014), enzymes (Willner *et al*., 2006), fungi (Vigneshwaran *et al*., 2007), and plants or plant extracts (Chandran *et al*., 2006, Song *et al*., 2009), have been recommended as possible eco-friendly substitutes to chemical and physical methods. Sometimes, the nanoparticle preparation using plants or parts of plants can prove advantageous over other biological processes, by eliminating the elaborate work involved in maintaining microbial cultures (Forough *et al*., 2011).

2.4.1 Co-precipitation

Magnetic nanoparticles of iron oxides magnetite (Fe_3O_4) or *maghemite* (γ-Fe_2O_3)can be synthesized through the co-precipitation of a stoichiometric mixture of Fe(II) and Fe(III) salts in a basic aqueous medium of sodium hydroxide (NaOH) or ammonium hydroxide (NH_4OH). Particles from 5 to 20 nm in diameter can be prepared by this synthesis method. Experimental conditions are critical and depend on the type of ion salt-chlorides, sulphates, nitrates orperchlorates and also on the Fe^{2+}/Fe^{3+} concentration ratio. Other synthesis parameters, such as pH, ionic force of the medium and reaction temperature, can be adjusted in the synthesis in order to control the size of magnetic iron oxide nanoparticles characteristics or surface properties (Wu *et al*., 2008; Gupta *et al*., 2005).

$$Fe^{2+} + 2Fe^{3+} + 8OH^- \rightarrow Fe(OH)_2 + 2Fe(OH)_3 \rightarrow Fe_3O_4 + 4H_2O$$

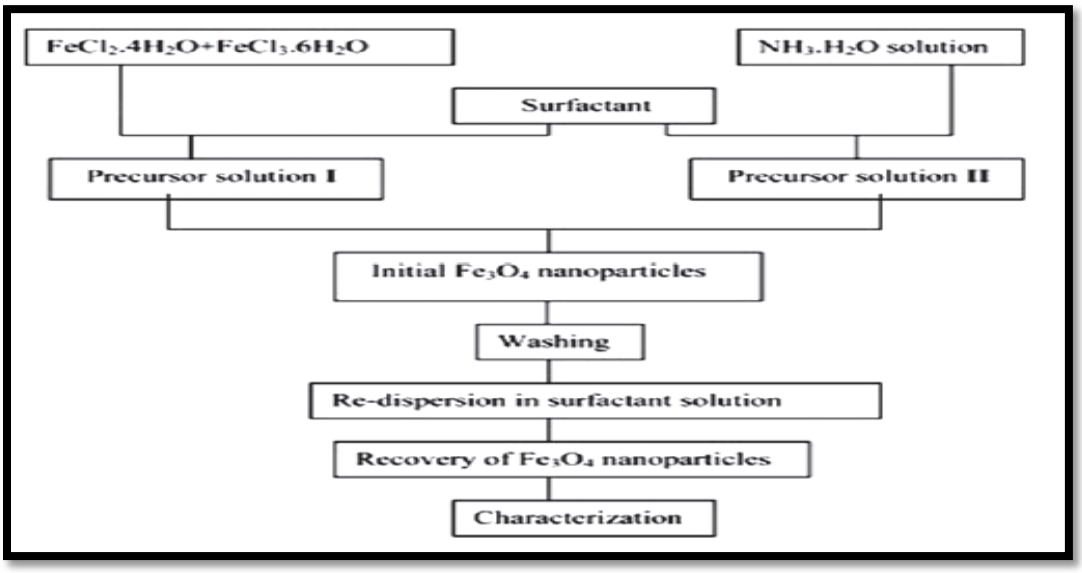

Figure 2: Procedure for the preparation of Fe_3O_4 NPs (Sun *et al*., 2007)

2.4.2 Microemulsion

Microemulsion is the thermodynamically stable isotropic dispersal of two immiscible water and oil phases in the presence of a surfactant. The surfactant molecules can form a monolayer at the interface between the oil and water, with the hydrophilic head groups in the aqueous phase and the hydrophobic tails of the surfactant molecules dissolved in the oil phase (Wu *et al*., 2008).This method has a series of advantages in comparison with other methods, namely, the use of simple equipment, the possibility of synthesizing a great variety of materials with a high degree of control over particle size and composition, the preparation of nanoparticles with crystalline structure and high specific surface area, and the use of simple conditions of synthesis, and near ambient temperature and pressure (Woo *et al*., 2004). Particles produced by the microemulsion method are smaller in size and are higher in saturation magnetization (Wu *et al*., 2008; Chin *et al*., 2007).

The properties of NPs prepared by the microemulsion method depend on the type and structure of the surfactant. The surfactant is an amphiphilic molecule which lowers the interfacial tension between water and oil, resulting in the formation of a transparent solution (Faraji *et al*., 2010).

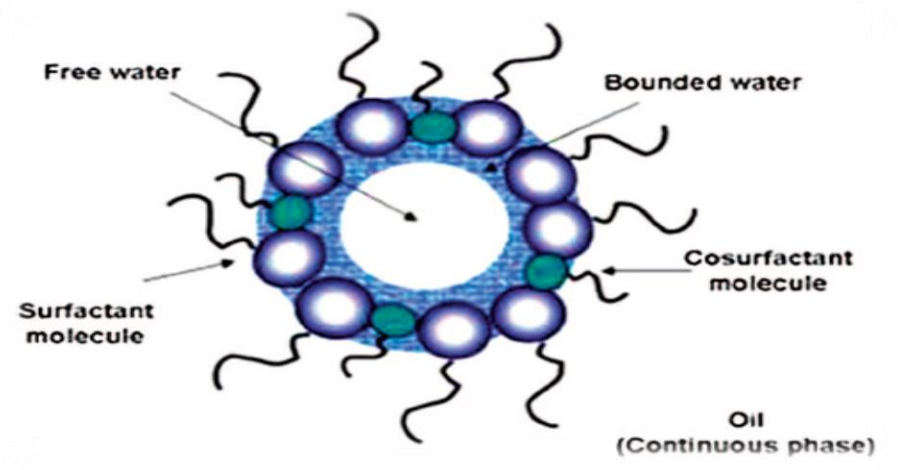

Figure 3: A schematic representation of water-oil microemulsion droplet (Moulik *et al*., 1998).

2.4.3 Thermal decomposition of organic precursors

The decomposition of iron precursors in the presence of hot organic surfactants has yielded improved samples with good size control, narrow size distribution, good crystallinity of individual and dispersible magnetic iron oxide NPs (Indira *et al*., 2010). Nanoparticles with a high level of monodispersity and size control can be achieved by high-temperature decomposition of organometallic precursors, such as $[M^{n+}(acac)_n]$, (M=Fe,Mn, Co, Ni, Cr; n =2 or 3, acac=acetylacetonate), M^x $(cup)_x$ (cup =N-nitrosophenyl hydroxylamine) or carbonyls (such as $Fe(CO)_5$), using organic solvents and surfactants such as fatty acids, oleic acid, and hexadecylamine (Faraji *et al*., 2010).

Biomedical applications like MRI are extremely dependent on particle size, and thus MNP synthesis by this method could be potentially used for these applications (Tartaj *et al*., 2003). The temperature and time of the reaction, as well as the aging period, may also be vital for the precise control of size and morphology (Lu *et al*., 2007). Laborious purification steps are essential before the end product can be used in biomedical applications (Eatemadi *et al*., 2014). The other disadvantage of this method is the production of organic-soluble nanoparticles,which limit the range of applications for their use in biological fields. In addition, surface treatment is needed after synthesis (Faraji *et al*., 2010); moreover, the resulting nanoparticles are generally only dissolved in non-polar solvents (Wu *et al*., 2008).

2.4.4 Hydrothermal and solvothermal synthesis

The aqueous solution route is used for the fabrication of α-Fe_2O_3 and Fe_3O_4 NPs; the solution synthesis for γ-Fe_2O_3 usually involved the controlled oxidation of Fe_3O_4 and the direct mineralization of Fe^{3+} ions. Subsequently, other non aqueous solution methods have also been developed to synthesize highly crystalline, monodisperse, and shape-controlled γ-Fe_2O_3 NPs, in which organometallic compounds were always used as precursors. However, hydrothermal or solvothermal synthesis includes various wet-chemical techniques of crystallizing the substance in a sealed container from the high temperature aqueous or non-aqueous solution (generally in the range 130-250^{0}C) under high vapor pressure (generally in the range 0.3-4 MPa) (Wu *et al*., 2008).

This method has also been used to grow dislocation-free single crystal particles, and grains formed in this process could have a better crystallinity than those from other processes, and hence hydrothermal and solvothermal synthesis are prone to obtaining highly crystalline IONPs, including α-Fe_2O_3, γ-Fe_2O_3, and Fe_3O_4 NPs.

Possible advantages of the hydrothermal method over other types of crystal growth include the ability to create crystalline phases which are not stable at the melting point. In addition, materials which have a high vapor pressure near their melting points can also be grown by the hydrothermal method (Laudise *et al*., 2004). The method is also particularly suitable for the growth of good-quality iron oxide nanocrystals while maintaining good control over their composition. It has to be pointed out that the concepts embodied in the hydrothermal process have already been extrapolated to non-aqueous systems, and the so-called 'solvothermal process' has emerged, in which an organic solvent is used as the reaction medium instead of water (Walton *et al*., 2002).

Moreover, the hydrothermal and solvothermal route is a facile and conventional method for obtaining hollow IONPs. Furthermore, the hydrothermal and solvothermal synthesis route has been developed to prepare IONPs with controllable size and shape (Cheng *et al*., 2012). In addition, the hydrothermal and solvothermal route is beneficial to obtaining shape-controlled IONPs. There are facile approach for the production of magnetic iron oxide short nanotubes (SNTs) and other shapes (nanoparticles, nanorings) employing an anion-assisted hydrothermal route by using phosphate and sulfate ions (Ji *et al*., 2012).

2.4.5 Sol-gel reactions and polyol method

The sol-gel process is a classical wet-chemical technique widely used in the fields of materials science and ceramic engineering. Such a method is used primarily for the fabrication of materials (typically metal oxides). Generally, it involves starting from a colloidal solution that acts as the precursor for an integrated network of either discrete particles or network polymers. In this system, a sol is a stable dispersion of colloidal particles or polymers in a solvent. A gel consists of a three dimensional continuous network, which encloses a liquid phase. In a colloidal gel, the network is built from the agglomeration of colloidal particles. In a polymer gel, the particles have a polymeric sub-structure made by aggregation of sub-colloidal particles.

Generally, sol particles may interact by Van der Waals forces or hydrogen bonds, and a gel may also form from linking polymer chains. In most gel systems used for materials synthesis, the interactions are of a covalent nature and the gel process is irreversible. The gelatin process may be reversible if other interactions are involved. Typical precursors for the synthesis of IONPs are iron alkoxides and iron salts (such as chlorides, nitrates and acetates), which undergo various forms of hydrolysis and polycondensation reactions (Pandey *et al*., 2011). These reactions are performed at room temperature, and further heat treatments are needed to acquire the final crystalline state. By this method, the IONPs will form through at least a two-step phase transformation: $Fe(OH)_3 \rightarrow \beta\text{-}FeOOH \rightarrow \gamma\text{-}Fe_2O_3$(Dong *et al*., 2002). The final properties of IONPs are highly dependent upon the structure created during the sol stage of the sol–gel process. The different organic precursors are the crucial roles in controlling the shape and crystal structure of IONPs.

The polyol method is also understood as an inversed sol-gel method (the sol–gel method uses an oxidation reaction but polyol synthesis uses a reduction reaction), which is well suited for the preparation of IONPs with various shapes and sizes (Laurent *et al*., 2008). In the polyol synthesis process, the polyols not only serve as solvents but also reducing agents, which apply as stabilizers to control particle growth and prevent interparticle aggregation. In the typical reaction process, an ironprecursor compound is suspended in a liquid polyol. The suspension is stirred and heated to a given temperature that can reach the boiling point of the polyol. Compared to the hydrothermal method, this reaction does not require high pressure, thus, it is unnecessary to operate in the Teflon-lined stainless steel autoclave (Cai *et al*., 2007). Polyol solvent also plays an important role in determining the size and magnetic properties of IONPs: different polyols will generate IONPs with different sizes (Caruntu *et al*., 2007; Shen *et al*., 2009).

In comparison with the co-precipitation method, the sol-gel and polyol methods for IONPs have several advantages. For example, the IONPs can be easily dispersed in aqueous media and other polar solvents because the surface of IONPs contains many hydrophilic ligands. Also the relatively high reaction temperature of these two methods favors IONPs with higher crystallinity and saturation magnetization. Never the less, the disadvantages of the sol-gel process are the relatively high cost of the metal alkoxides and the release of large amounts of alcohol during the calcination step, requiring safety considerations during the sol-gel process.

2.4.6 Sonochemical reactions

The sonochemical method has been widely used as a competitive alternative to synthesize novel materials with unusual properties (Wu *et al*., 2008, Faraji *et al*., 2010). The chemical effects of ultrasound arise from acoustic cavitations, that is, the generation, growth, and implosive collapse of bubbles in liquid. The conditions designed in the hotspots which are formed by the implosive collapse of the bubble, show temporary temperatures of 5000 K, pressures of 1800 atm, and cooling rates in excess of 10 K/s (Wu *et al*., 2008). Figure 4 illustrates the common steps of iron oxide synthesis by the sonolysis method.

Commonly, volatile precursors in solvents of low vapor pressure are used to improve the particle yield. Acoustic irradiation is carried out with an ultrasound probe, such as a titanium horn, operating at 20 kHz (Willard *et al*., 2004). This method has been applied for the synthesis of several nanocomposites, and its versatility has been successfully confirmed in iron oxide NP synthesis (Bang *et al*., 2007).

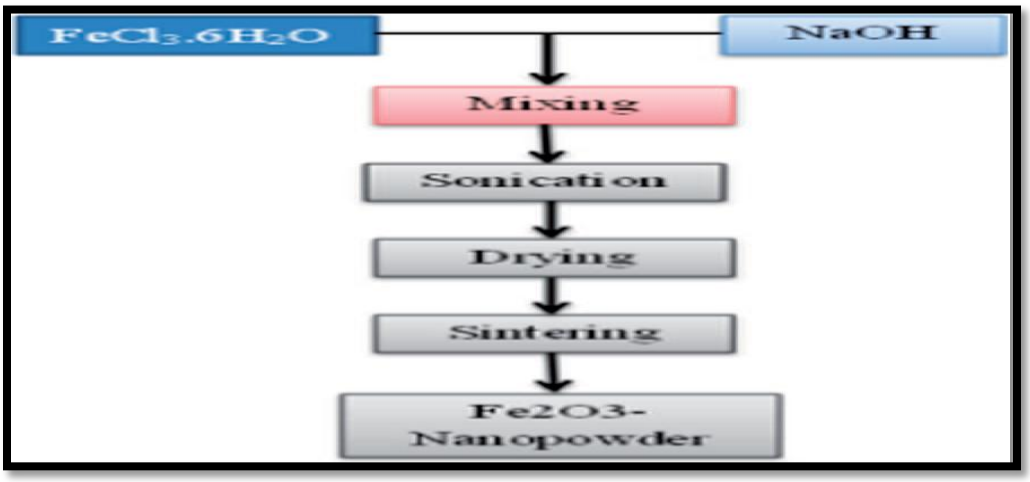

Figure 4: Flow chart of the sonochemical synthesis of iron oxide (Ashokkumar *et al*., 2007).

2.4.7 Microwave-assisted synthesis

It has long been known that molecules undergo excitation with electromagnetic radiation. This effect is utilized in household microwave ovens to heat food. However, microwave-assisted synthesis has only been used as a reaction methodology by chemists for a few years. Excitation with microwave radiation results in the molecules aligning their dipoles within the external field. Strong agitation, provided by the reorientation of molecules, in phase with the electrical field excitation, causes an intense internal heating. Therefore, microwave-assisted synthesis can significantly reduce the processing time and energy cost, due to its almost instantaneous 'in core' heating of materials in a homogeneous and selective manner, different from the classical ones. The microwave-assisted synthesis method has been widely used to prepare magnetic IONPs with controllable size and shapes recently (Wu *et al*., 2011; Ai *et al*., 2010; Qiu *et al*., 2011).

Indeed, the phase of IONPs by the microwave-assisted synthesis could be slightly different depending on the experimental conditions (Hu *et al*., 2011). Additionally, the microwave-assisted synthesis method is often employed to prepare biocompatible magnetic IONPs (Osborne *et al*., 2012).

Compared to the thermal decomposition method, the stabilization of the IONPs prepared by the microwave-assisted synthesis route in organic solvents can be easily dispersed in water without laborious ligand exchange or purification steps. Such characteristics can be considered as attractive for fabrication of large-scale IONPs (Pascu *et al*., 2012).

2.5 Green synthesis of metal NPs

Green nanotechnology has attracted a lot of attention and includes various processes which decrease or eliminate toxic substances to restore the environment. The biosynthesis of metal nanoparticles by plants is currently under development. The synthesis of metal NPs using inactivated plant tissue, plant extracts, exudates, and other parts of living plants, is a modern option for their production (Pourhassan-Moghaddam *et al*., 2014). Green synthesis of NPs makes use of environmentally friendly, non-toxic and safe components. The development of reliable, nontoxic, and eco-friendly methods for the synthesis of NPs is of extreme importance to develop their biomedical applications (Salam *et al*., 2012, Mahdavi *et al*., 2013).

Green biosynthesis of nanoparticles employs the bottom-up approach where the metal atoms assemble to form clusters and then eventually the nanoparticles. The biological compounds present in green materials may act as both reducing and capping agents that can stabilize the nanoparticles during the synthesis process. This can control the size and shape of the nanoparticles which can be used in various applications. Figure 5 shows the simple process of nanoparticles synthesis where the materials needed are metal salt (precursor) and green substrate only. Various parameters such as concentration of metal salt, concentration of green substrate, time and temperature for reaction and pH of the solution can be altered during the nanoparticles synthesis process in order to obtain properties that are needed for respective applications (Yew *et al*., 2018).

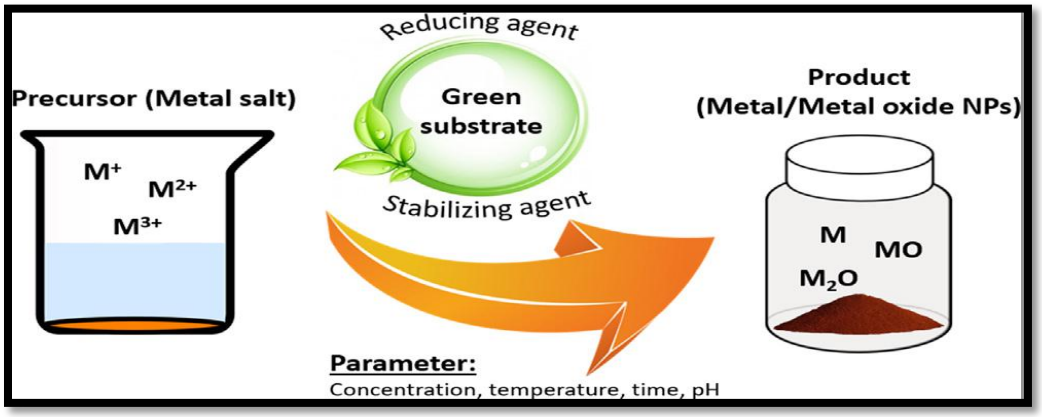

Figure 5: Nanoparticles green synthesis process.

The reason for selecting plants for biosynthesis is due to their reducing agents such as citric acid, ascorbic acids, flavonoids, reductases, dehydrogenases and extracellular electron shuttles, which may play an important role in the biosynthesis of MNPs (Pandey *et al*., 2012).

Some of the distinct advantages that biological synthesis protocols have over the conventionally used physical and chemical methods are: clean and eco-friendly method, toxic chemicals are not used; the active biological component like enzyme can acts as a reducing and capping agent, thereby reducing the overall cost of the synthesis process; small nanoparticles can be produced even during large-scale production; external experimental conditions like high energy and high pressure are not required, causing significant energy saving (Mihir *et al*., 2014).

2.5.1 Green synthesis using plant leaf extract

The green synthesis of iron oxide nanoparticles using various plant extracts has been reported by many researchers. Rapid synthesis of iron oxide nanoparticles is performed by reduction of ferric and ferrous salts ($FeCl_3$, $FeSO_4$) with leaf extract of different plants. The preparation steps are very simple where the ferrous and ferric salts are added to the leaf extract. The paste form sample is calcinated at 700^0C for 1h to remove all the impurities. The leaf extract of the plant contains water soluble carbohydrate compounds. Carbohydrates containing aldehyde groups may reduce the Fe^{3+} of ferric chloride to Fe_3O_4 nanoparticles (Senthil *et al*., 2012; Prasad *et al*., 2016).

2.5.2 Green synthesis using plant fruit extract

Some researchers use fruit extract for synthesis of iron oxide nanoparticles. Stable iron oxide nanoparticles are synthesized via simultaneous reduction of $FeSO_4.7H_2O$ solution by fruit extract containing complexation of polyphenols (MohanKumar *et al*., 2013).

In another study spherical magnetic iron oxide nanoparticles (Fe_3O_4) synthesis from the aqueous fruit extract of *Passifloratripartitavarmollissima* and their catalytic effect on the synthesis of 2-arylbenzimidazole under room temperature is studied (Kumar *et al*., 2014).

2.5.3 Green synthesis using plant seed extract

Iron oxide nanoparticles are synthesized using seed extract of *Syzygiumcumini* as a reducing agent and sodium acetate as an electrostatic stabilizing agent. The XRD study reveals that the synthesized spherical magnetic nanoparticles (SMNPs) have inverse spinel face-centered cubic structure 9-20 nm in diameter as shown by TEM. The presence of polyphenols, flavonoids, and other biomolecules in the *S. cumini* seed is confirmed by Fourier transform infrared (FTIR) spectroscopy technique. The Brunauer-Emmett-Teller (BET) surface area of the Fe_3O_4 particles is found and the particles are classified as mesoporous. The average pore size for the Fe_3O_4 is determined according to the single-point adsorption total volume at a relative pressure P/P_o. By virtue of this property, the synthesized nanoparticles are used in the field of environmental remediation for the removal of toxic metals and dyes (Venkateswarlu *et al*., 2014).

2.5.4 Green synthesis using plant peel extract

The facile green synthesis of magnetite nanoparticles is performed by using waste plantain peel extract for reduction of iron salt to form Fe_3O_4 nanoparticles. Biomolecules present in the plantain peel extract is characterized by FTIR. The well dispersed spherical magnetic nanoparticles size is seen in a transmission electron microscopic (TEM) image. Magnetic nanoparticles have excellent magnetic behavior and on the basis of BET surface area and pore volume results, the structure of nanoparticles is assigned to be mesoporous. By virtue of this property, synthesized nanoparticles are used in the field of environmental remediation for the removal of toxic metals and dyes (Venkateswarlu *et al*., 2013).

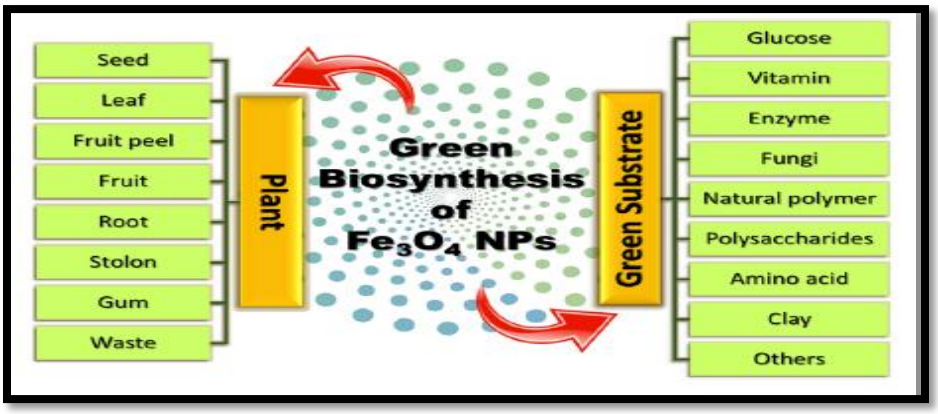

Figure 6: Materials of green biosynthesis of Fe_3O_4 NPs (Yew *et al*., 2018).

2.6 Mechanism for synthesis of iron oxide nanoparticles through green synthesis method

The presence of biomolecules or combinations of chemically complex biomolecules, such as enzymes, proteins, vitamins, polysaccharides, polyphenols, flavonoids, terpenoids, aldehydes, amides and organic acids such as citrates, tannic acids, ascorbic acids, amino acids, carboxylic acids and many reducing sugars are commonly found in plants and may act as reducing and capping agents in nanoparticle synthesis (Iravani *et al*., 2011).

Phytochemicals in plant extracts possess ideal redox properties that allow efficient reduction of metal precursors for conversion into their corresponding metallic nanoparticles. Tannin powder, For example is used as a green reagent for synthesis of iron oxide nanoparticles. It consists of non-toxic polyphenolic compounds which act as reducing and stabilizing agents for the production of iron oxide nanoparticles. The presence of phenolic-OH groups and ortho-dihydroxyphenyl groups in chemical structure of tannins are involved in the formation of complexes with iron and also take part in redox reactions. In the formation of iron oxide nanoparticles by tannins, the reactions undergo changes in electron structure. Tannins are oxidized to quinines and associated to derivate into radical tannins "R" which causes reduction of metal (iron) under the influence of pH and by this reaction; iron salt is reduced to iron oxide nanoparticles (Herrera *et al*., 2010).

The bioreduction mechanism process is written as:

$$FeCl_3 + H_2O \longrightarrow [Fe(H_2O)_n]^{3+} + H_2O \quad (1)$$

$$R + [Fe(H_2O)_n]^{3+} + H_2O \longrightarrow [Fe(H_2O)_n]^{2+} + H^+ + R\text{–}OH \quad (2)$$

$$[Fe(H_2O)_n]^{2+} + 2R^- + H^+ + OH^- + pH \longrightarrow Fe^{2+}O^{2-} + Fe^{2+}Fe^{3+}O^{2-} + R\text{–}H + R\text{–}OH^- \quad (3)$$

2.7 Potential applications of magnetite (Fe_3O_4) nanoparticles

Iron oxide nanoparticles are significantly important for abatement of environmental pollution such as degradation of organic dyes, chlorinated organic pollutants, heavy metals removal, targeted drug delivery, magnetic resonance imaging, magnetic hyperthermia, thermoablation, bioseparation and biosensing. Recent developments on the use of magnetite nanoparticles and magnetite containing composite nanomaterials for the removal of heavy metals from wastewaters are presented.

Iron oxide nanoparticles have been intensively developed not only for its fundamental scientific interest but also for many technological applications: such as ferrofluids for audio speakers, and magnetic recording media. Green biosynthesized Fe_3O_4NPs can possess better characteristics, such as higher biocompatibility and biodegradability, compared to physically synthesized Fe_3O_4 NPs.

Hence, they can be utilized in biomedical application due to the special surface coating of green materials, which is not only non-toxic and biocompatible yet also allow targeted drug delivery withFe_3O_4 NPs localization at particular area. Toxicity towards human body can be minimized because the green materials used for synthesizing Fe_3O_4 NPs are safe to be consumed, and thus it would be beneficial in biomedical applications. Besides, Fe_3O_4 NPs can conjugate with drugs, enzymes or proteins which can be directed to targeted tissue, organ or tumor with the aid of external magnetic field or can be heated in alternating magnetic fields for hyperthermia treatment (Mahdavi *et al*., 2013).

Figure 7 shows the possible applications of Fe_3O_4 NPs used in the fields of catalyst, water remediation (heavy metal ion removal), lithium ion battery, magnetic storage media. All these give promising results and provide a platform for Fe_3O_4NPs which their unique features offer tremendous potential for their vast application ((Ghandoor *et al*., 2012; Venkateswarlu *et al*., 2014).

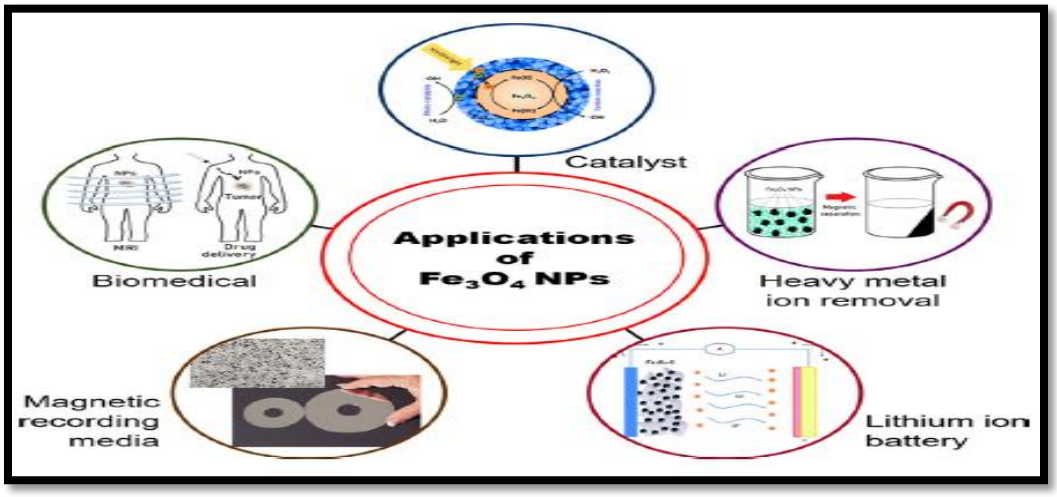

Figure 7: Applications of Fe_3O_4 NPs

2.7.1 Magnetite (Fe_3O_4) nanoparticles for Antibacterial Activity

Various studies confirm that iron nanoparticles possess good antimicrobial properties.The antibacterial effect of *TridaxProcumbens*synthesised iron oxide (Fe_3O_4) nanoparticles wasinvestigated by Senthil and Ramesh (Senthil*et al*., 2012) against gram negative bacteria *Pseudomonas aeruginos*.

The reactive oxygen species (ROS) generated by Fe_3O_4 nanoparticles could kill bacteria without harming nonbacterial cells. Specifically, Pareta *et al*; cultured *osteoblasts* (bone-forming cells) with Fe_3O_4nanoparticle and found that cell density was greatly enhanced in the presence of Fe_3O_4nanoparticles compared with cells cultured without nanoparticles. This suggests that the Fe_3O_4 NPs combined with conventional antibiotics can exert synergistic effect, which reduce the doses of antibiotics and thus decrease the phenomenon of resistant bacterial and mammalian cell toxicity (Patra *et al*., 2017).

2.7.2 Magnetite (Fe_3O_4) nanoparticles for heavy metal ions removal

Nowadays, there is a continuously increasing worldwide concern for the development of wastewater treatment technologies. Great attention has been paid to the effective removal of heavy metal ions, especially highly toxic heavy metals such as chromium, mercury, arsenic, cadmium, copper, lead and zinc from the environment. Different treatment technologies are available for the removal of toxic heavy metals. The adsorptions, chemical precipitations, ion exchange, coagulation, reverse osmosis, electrolysis and membrane process are widely used. However, among all these methods, adsorption is considered as one of the most effective, efficient and economical method for the removal of pollutants from wastewater (Ilankoon *et al*., 2014).

The utilization of iron oxide (Fe_3O_4) nanoparticles as the adsorbents has been received much attention due to their unique properties, such as high surface area-to-volume ratio, surface modifiability, excellent magnetic properties, good biocompatibility, ease of separation using external magnetic field, reusability and comparatively low cost. Therefore, negatively charged ligands, electrolytes, and other suspended particles will undergo interaction (adsorption) with magnetite's active surface sites (Dave *et al*., 2014).

2.7.3 Dye-sensitized solar cell application

Dye-sensitized solar cells (DSSCs) have received widespread attention due to their high efficiency, low cost and simple preparation over the last 20 years. Typically, DSSCs consist of a dye-sensitized porous TiO_2photoanode, an electrolyte containing the iodide/tri-iodide redox couple, and a platinized counter electrode. Among these parts, the photoanode properties are critical to determine the efficiency of DSSCs. Most recent studies of the photoanode have been focused on optimizing materials and structures for improving the performance of DSSCs (Kang *et al*., 2015).

Recently, magnetic field effects have drawn strong interest because of their wonderful potential applications ranging from catalysis to electronics and energy. Applying a weak external magnetic field was explored as an alternative strategy for enhancing the short circuits current (*Jsc*) and light conversion efficiency of solar cells (Hu *et al*., 2011).

Magnetic γ-Fe_2O_3 nanoparticles are dispersed in TiO_2 film with the intention of improving the efficiency of DSSCs. The power conversion efficiency of the DSSCs can be increased at an optimal amount of γ-Fe_2O_3 nanoparticles compared with the cell with pure TiO_2 nanoparticles. The solar cell performance increased without changing the thickness and the complexity of the device. This increase is attributed to the effect of the magnetic field generated from γ-Fe_2O_3 nanoparticles, leading to improved photo generated electron transfer ability, increased separation efficiency of charges, and reduced charge recombination (Fengshi *et al*., 2015).

3. MATERIALS AND METHODS

3.1 Materials

3.1.1 Chemicals and Solvents

The following chemicals and solvents were used in this study. Ferric chloride hexahydrate ($FeCl_3.6H_2O$, MW= 270.30 g/mol; Blulux Ltd, India), ferrous chloride tetrahydrate ($FeCl_2.4H_2O$, MW =198.81 g/mol; Atico, India), Potassium dichromate ($K_2Cr_2O_7$, MW = 294.18 g/mol; Blulux Ltd, India), Mercury (II) chloride ($HgCl_2$, MW = 271.50 g/mol; Blulux Ltd, India), Sodium hydroxide (NaOH, M.W = 39.99971 g/mol; Blulux Ltd, India), Ethanol (99.9%; Blulux Ltd, Ranchem Industry and Trading), HCl, H_2SO_4, $KMnO_4$, Diphenylcarbazide (DPC) and distilled water were purchased.

3.1.2 Apparatus and instrumentation

The laboratory apparatus and instruments used for this study were the following: Whatmann filter paper, ordinary filter paper, Erlenmeyer flask, volumetric flask, measuring cylinder, magnetic stirrer, drying oven, muffle furnace, centrifuge, digital electronic balance, ultrasonic bath, glass filters, beakers, test tubes, borosilicate glass, mortar and pestle, pH metre, micro grinding machine, hot plate, pipets, spatulas, plastic bottles, thermometers, aluminum foils, TGA, XRD, FT-IR, SEM, EDS and UV-Vis spectroscopic techniques.

3.2 Methods

3.2.1 Collection of plant material

Fresh, matured, disease free and healthy *Thymus schimperi* leaves were collected from Arsi Zone after conducting field surveys. The collected *Thymus schimperi* leaves (Figure 8) were used to make the aqueous extracts.

Figure 8: Pictures of leaves of Thymus schimperi taken from East Arsi Zone Chilalo Mountain (By Sintayehu Tammane Geneti)

3.2.2 Preparation of *Thymus schimperi* leaf extract

The plant leaves were thoroughly washed several times with running tap water and then rinsed with distilled water. The surface water was allowed for air dry at room temperature. The dried plant leaves were then cut into small pieces and about 10g was weighed for extraction. The aqueous extract of sample was prepared by boiling the freshly collected cut leaves (10g) with 200 mL of distilled water, at 80^0C for about 60 minutes by stirring well until the color of the aqueous solution changes from watery to light brown. The aqueous extract of sample was cooled to room temperature and filtered first with ordinary filter paper and then using whatmann filter paper. Then the filtrate extract was stored in a refrigerator at 4^0C for further experiments (Sravanthi *et al*., 2016).

Figure 9 (a-e) shows washed and dried, small cut pieces, cut leaves boiled, first filtration and filtrate extract of *Thymus schimperi* preparation processes respectively.

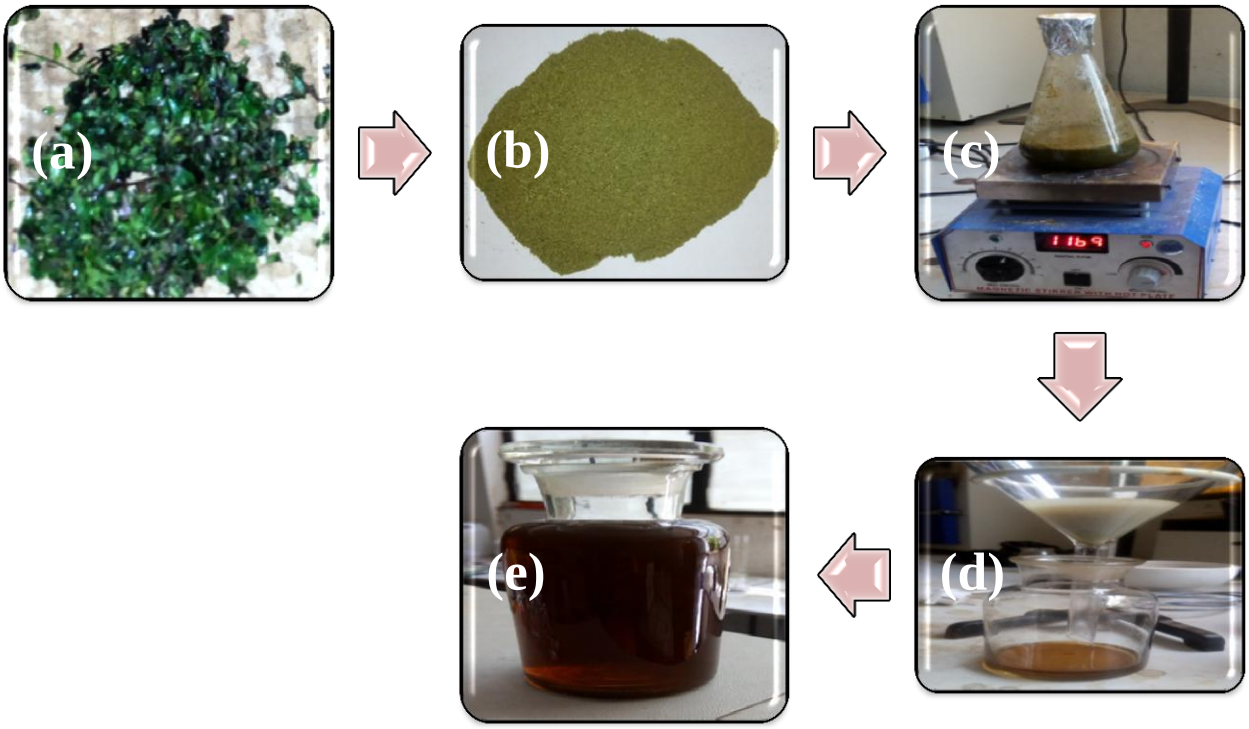

Figure 9: *Thymus schimperi* leaf extract preparation processes.

3.2.3 Preparation of precursor salt solution

Ferric chloride ($FeCl_3.6H_2O$) and ferrous chloride ($FeCl_2.4H_2O$) salts solution was used as precursor for the synthesis of Fe_3O_4 NPs using aqueous extract of *Thymus schimperi* leaf extracts. $FeCl_3.6H_2O$ (0.1M) and $FeCl_2.4H_2O$ (0.05M) precursor solution was prepared by mixing 13.6g of $FeCl_3.6H_2O$ and 5g of $FeCl_2.4H_2O$ salts and dissolving the mixture in 500mL of distilled water in 1000mL volumetric flask followed by stirring in room temperatures for about 15 minutes (Figure 10) and then stored for further use. 2M NaOH was prepared using distilled water which was used as precipitating agent. Then three different samples were prepared by taking different ratios by volume of precursor salts solution to *Thymus schimperi* leaf extract.

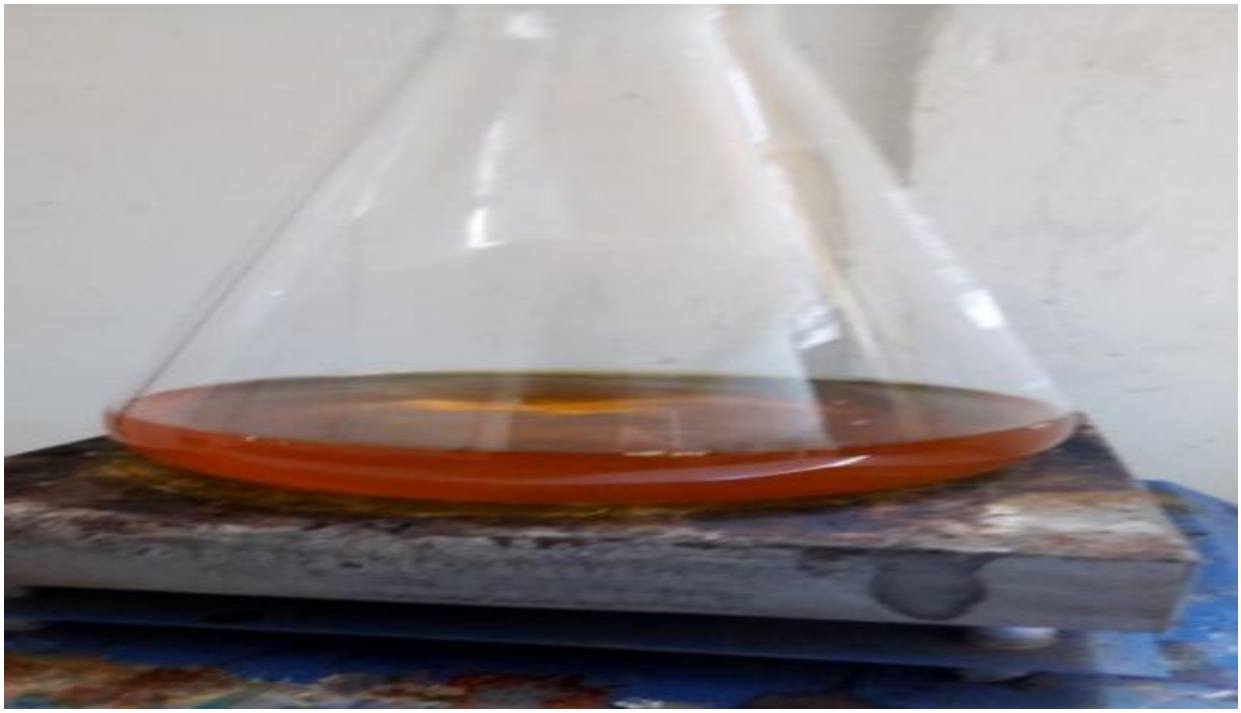

Figure 10: Ferric chloride and ferrous chloride precursor salt solution

3.2.4 Biogenic synthesis of Fe_3O_4 NPs

In a typical experiment, the extract was added to ferric chloride and ferrous chloride precursor solution in three different ratios by volume.

Sample 1: Precursor salt solution: Leaf Extract in 2:1 ratio by volume labeled as **S21**
Sample 2: Precursor salt solution: Leaf Extract in 1:1 ratio by volume labeled as **S11**
Sample 3: Precursor salt solution: Leaf Extract 1:2 ratios by volume labeled as **S12**

Possible reaction mechanism is written as:

$$2FeCl_3.6H_2O + FeCl_2.4H_2O + 8NaOH + \text{Plant extract} \longrightarrow Fe_3O_4 + 8NaCl + 20H_2O + \text{Byproduct}$$

50 mL of the extract was added to 100 mL of the precursor solution with 2M NaOH for S21 preparation in one 250mL conical flask.

100 mL of the extract was added to 100 mL of the precursor solution with 2M NaOH for S11 preparation in the second 250 mL conical flask.

100 mL of the extract was added to 50 mL of the precursor solution with 2M NaOH for S12 preparation in the third 250 mL conical flask.

Then for each sample the mixtures were stirred continuously at 60^0C for 1 hour with magnetic stirrer and resulted in solution with black precipitate. The precipitate was filtered using Whatman filter paper No 1 and washed repeatedly with distilled water followed by ethanol in order to remove the impurities. Finally, the precipitate was dried in an oven at 60^0C for one hour and grinded to fine powder. The black powder obtained from the above method was calcined at 700^0C for 1 hour (Herleka r*et al*., 2015). The sample was then labeled for further uses.

Figure 11 shows Fe_3O_4 NPs synthesized from *Thymus schimperi* leaf extracts with hydrated ferric and ferrous chloride precursor.

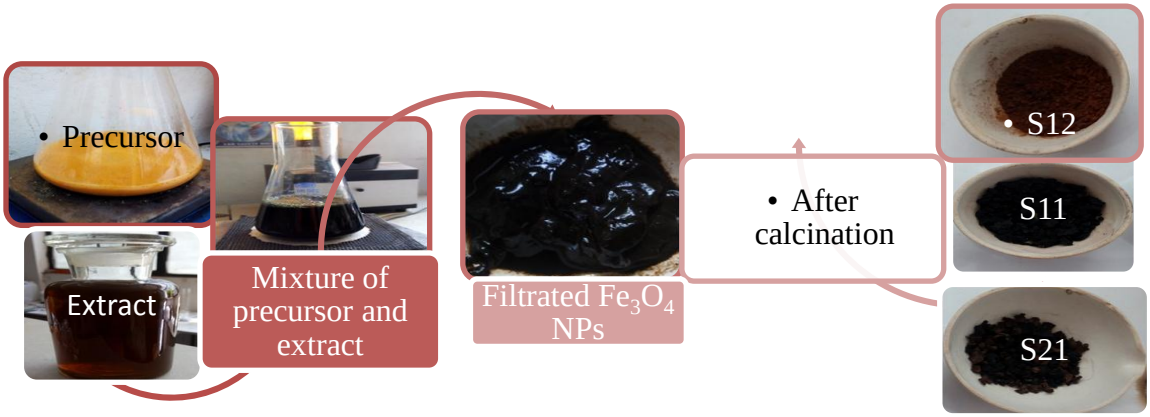

Figure 11: Schematic diagram of synthesis processes for Fe_3O_4 NPs

3.3 Characterization Techniques of Green Synthesized Fe_3O_4 NPs

3.3.1 Thermo gravimetric analysis (TGA)

Thermal gravimetric analysis (TGA) was carried out using a simultaneous DTA-TGA apparatus (DTG-60H, Shimadzu Co., South Korea) in order to decide the calcination temperature of the synthesized Fe_3O_4 nanoparticles. About 19.073 mg of the uncalcinated magnetite (Fe_3O_4) nanoparticles of samples powder were placed in a platinum crucible on the pan of the microbalance and heated from room temperature to about 700^0C (Herlekar *et al*., 2015), using platinum as inert material.

3.3.2 Characterization using x-ray diffraction (XRD) technique

A small amount of the powder was taken and the crystalline structures of the green synthesized Fe_3O_4 nanoparticles were investigated by the X-ray diffraction using X-ray diffractometer (XRD-7000 X-Ray diffractometer, Shimadzu Co., South Korea). In this XRD analysis the powder of synthesized Fe_3O_4 NPs were used. XRD spectrum was recorded from 10^0 to 80^0 with 2θ angles using CuKα (λ=1.54 Å) radiation operated at 40kV and 30 mA. Debye Scherrer's equation indicated in equation below, was used to estimate the crystallite size (Ghandoor *et al*. 2012).

$$D = \frac{0.94\,\lambda}{\beta cos\theta} \tag{3.1}$$

Where, D is the Crystallite size, λ is the X-ray wavelength (1.5406 Å), β is the Full Width at Half Maximum (FWHM) of a peak, and θ is the peak position.

3.3.3 Characterization using Fourier transforms infrared (FTIR) technique

Fourier transform infrared spectroscopy (FTIR) spectra of the synthesized Fe_3O_4 NPs were recorded at room temperature using a FTIR spectrophotometer in order to analyze and detect surface functional groups at the scanning range of 4000-400 cm^{-1}. For FTIR measurements, a small amount of powdered synthesized Fe_3O_4 NPs was mixed with KBr and a pellet was prepared for FTIR spectral analysis (Awwad *et al*., 2012).

3.3.4 Characterization using SEM-EDS techniques

SEM-EDX analysis reveals information about the sample including external morphology, chemical composition and crystalline structure and orientation of materials making up the sample. SEM provides detailed images of the sample by rastering a focused electron beam across the surface and detecting secondary or back scattered electron signal. The chemical composition of the synthesized Fe_3O_4 NPs was estimated by energy dispersive X-ray (EDS) spectroscopy (Chen *et al*., 2013; Santos *et al*., 2012).

3.3.5 Characterization using UV-Vis spectroscopy

The UV-Vis absorption spectra of the biosynthesized Fe_3O_4 NPs was confirmed by using a wavelength scan between 200 nm and 800 nm. From the synthesized Fe_3O_4 NPs, a small amount of the sample was taken and characterized by using UV-Vis spectrometer. This characterization technique gives information about the optical properties of NPs (Basavegowda *et al*., 2014). The optical reflection spectrum of Fe_3O_4 NPs depends on the particle size, shape, state of aggregation and the surrounding dielectric medium (Petla *et al*., 2012).

3.4 Preparation of Metal Solutions

3.4.1 Preparation of chromium (VI) and mercury (II) solutions

The stock solutions of Cr(VI) and Hg(II) were prepared by dissolving 2.826 g of analytical grade of $K_2Cr_2O_7$ and 1.354 g of analytical grade of $HgCl_2$ in 1 L of distilled water respectively. The stock solutions were further diluted with distilled water to obtain the desired concentration of standard solutions for absorbance measurement. The initial pH of the test solutions were adjusted to the desired value (pH = 3) by using dilutes solutions of HCl and NaOH. The required lower concentrations were prepared by dilution of the stock solutions. All precautions were taken to minimize the loss due to evaporation during the preparation of solutions and subsequent measurements. The stock solutions of chromium and mercury were prepared fresh for each experiment as the concentration of the stock solutions may change on long standing.

3.4.2 Preparation of diphenylcarbazide (DPC) solution

1, 5-diphenylcarbazide was used for spectrophotometric determination of Cr(VI). Diphenylcarbazide (DPC) solution was prepared by dissolving 25mg of DPC in 50 ml of acetone in a 100 ml volumetric flask for color development of the metal ions solution after adsorption. Standard solutions were prepared by diluting a 20mg/L Cr(VI) stock solution with 0.2M H_2SO_4 and 1 mL of DPC solution and linear calibration curves were obtained (Padmavathy *et al.*, 2016).

3.4.3 Preparation of potassium permanganate ($KMnO_4$) solution

Potassium permanganate ($KMnO_4$) solution was prepared by dissolving 25mg of $KMnO_4$) in 50 ml of distilled water in 100 ml volumetric flask for color development of the metal ions solution after adsorption. Standard solutions were prepared by diluting a 20mg/L Hg(II) stocksolution with 0.2M H_2SO_4 and 1 mL of $KMnO_4$solution and linear calibration curves were obtained(Mohd *et al*., 2013).

3.5 Analysis of standard curves for chromium (VI) and mercury (II) standard solutions

2 mL of 0.2M H_2SO_4 was added to 15 mL of standard samples containing known concentration of chromium and mercury and pH was adjusted using 0.1M HCl and 0.1M NaOH. The solution was mixed well and then diluted in a volumetric flask using distilled water. Further 1 mL of DPC solution was added to chromium solution and 1 mL of potassium permanganate was also added to mercury solution and then mixed well. Full colour development for these two solutions was formed and after 10 min, 4 mL of these solutions was used in an absorbance measurement cell (cuvette) and the concentrations were measured spectroscopically at 540nm for chromium solution (Padmavathy *et al.*, 2016) and at 253.7nm for mercury solution in UV spectrophotometer (Mohd *et al*., 2013).

3.6 Batch adsorption study

Batch adsorption studies were conducted to investigate the efficiency of magnetite (Fe_3O_4) nanoparticles for the removal of chromium (VI) and mercury (II) ions from aqueous solutions. All experiments were conducted at room temperature 25^0C (±0.5). The desired pH of the solution was adjusted by using 0.1M NaOH and 0.1M HCl. A known amount of adsorbent was added to samples and agitated by a shaker at 100 rpm agitation speed, allowing sufficient time, 90 min for adsorption equilibrium. The extent of chromium and mercury ions removal was investigated separately by changing adsorption dose (100mg, 300mg, 500mg and 700mg), contact time (30 min, 60 min, 90 min and 120 min), initial concentration (20mg, 40mg, 60mg and 80mg) and pH of the solution (3, 5, 7, 9 and 11). After adsorption, the adsorbent was separated from the solutions using a filter paper and the initial and final metal concentrations were determined. The equilibrium adsorption capacity *(Qe)* was calculated according to the following equation,

$$Q_e = \left(\frac{Co - Ce}{M}\right)V \qquad (3.2)$$

Where *Qe* is the equilibrium adsorption capacity (mg/g), C_0 and *Ce* are the initial and equilibrium liquid phase solute concentration (mg/L), respectively; V is the liquid phase volume (L) and M is the amount of adsorbent (g).

The maximum heavy metals percent removal (%) was calculated using the equation:

$$Removalpercent(\%) = \frac{Co - Ce}{Co}\ x\ 100 \qquad (3.3)$$

Where C_o is the initial concentration and *Ce* is the concentration at equilibrium after treatment with adsorbent. Optimum period of time to achieve maximum percent removal was determined.

3.6.1 Sorption kinetics

Kinetic studies are significant for any kind of sorption processes. Adsorption kinetics not only describes the adsorption mechanism of metals on adsorbents but also describe the metal adsorption rate which controls the contact time of metals at the solid-liquid interface. The adsorption mechanism depends on the physical and chemical characteristics of adsorbent and adsorbate, pH of medium, temperature, contact time and aids and mass transport process. Adsorption kinetics is performed to evaluate both the equilibrium time and the rate of Cr(VI) and Hg(II) adsorption. The equilibrium time is one of the important parameters for subsequent adsorption isotherm studies.

To evaluate the rate of Cr(VI) and Hg(II) adsorption on adsorbents, the experimental data was analyzed using pseudo first and pseudo second order kinetic models. The pseudo second order model is commonly used to describe chemical adsorption process of pollutants from aqueous solutions in recent years. Linear regressions are frequently used to determine the best fitting kinetic models, and the method of least squares is used for finding parameters of the kinetic model (Ya *et al*., 2011).

3.6.2 Sorption Isotherm Models

Sorption isotherm is an empirical relationship used to predict how much solute can be adsorbed by the adsorbent. Adsorption isotherm is defined as a graphical representation showing the relationship between the amount adsorbed by a unit weight of adsorbent and the amount of adsorbate remaining in a test medium at equilibrium, and it shows the distribution of adsorbable solute between the liquid and solid phases at various equilibriums.

The purpose of the adsorption isotherms is to relate the adsorbate concentration in the bulk and the adsorbed amount at the interface or to describe distribution of metal ions between the liquid phase and the solid phase. The isotherm results were analyzed using the Langmuir (Langmuir *et al*., 1916) and Freundlich (Freundlich *et al*., 1906).

3.6.2.1 Langmuir isotherm model

The Langmuir adsorption model is based on the assumption that maximum adsorption corresponds to a saturated monolayer of solute molecules on the adsorbent surface, with no lateral interaction between the sorbed molecules or that the uptake of metal ions occurs on a homogenous surface by monolayer adsorption without any interaction between adsorbed ions. The Langmuir adsorption isotherm has been successfully used to explain the adsorption Cr(VI) and Hg(II) from solutions(Padmavathy *et al.*, 2016; Mohd *et al*., 2013). In the Langmuir model, adsorption increases with increasing solute concentration at low concentration values and approaches a constant value at high concentrations because there are a limited number of adsorption sites in the nanosorbent. The expression of the Langmuir model is given by

$$q_e = \frac{Q_o b C_e}{1 + bC_e} \tag{3.4}$$

Where, q_e (mg/g) and C_e (mg/L) are the amount of adsorbed Chromium and mercury per unit mass of sorbent and unadsorbed chromium and mercury concentration in solution at equilibrium, respectively. Q_0 is the maximum amount of chromium per unit mass of sorbent to form a complete monolayer on the surface bound at high C_e, and b is a constant related to the affinity of the binding sites (L/mg)(Langmuir *et al*., 1918).

3.6.2.2 Freundlich isotherm model

The model is based on the assumption that ions are accumulated infinitely on the sorbent surface. The Freundlich isotherm equation may also be given as:

$$q_e = KC_e^{1/n} \tag{3.5}$$

Where, 1/n (mg/L) is adsorption intensity and K constant related to the adsorption energy (mol^2/KJ^2). However, the Freundlich model assumes that the uptake of metal ions occurs on heterogeneous surface by monolayer adsorption (Freundlich *et al*., 1906). In order to find the most appropriate model for the chromium and mercury adsorption, the data were fitted to each isotherm model.

4. RESULTS AND DISCUSSION

4.1 Thermo Gravimetric Analysis (TGA) Result

The uncalcinated synthesized Fe_3O_4 nanoparticles using $FeCl_3.6H_2O$ and ferrous chloride $FeCl_2.4H_2O$ salts precursor and *Thymus schimperi* extract was characterized by using TGA/DTA (Differential Thermal Analysis) and heated from room temperature to about 700^0C (Herlekar*et al*., 2015), using platinum as inert material. The weight losses of the investigated materials were analyzed. Figure 12 shows the thermo gravimetric analysis (TGA) and differential thermal analysis (DTA) of the uncalcined Fe_3O_4 NPs. TGA curve shows mass loss of the sample whereas DTA curve indicates the energy gain or loss during the process. TGA/DTA transition on the temperature range up to 450^0C a weight loss of 27.694 % was observed. No considerable loss was observed after this up to 450^0C. TGA-DTA data for $FeCl_3.6H_2O$ and $FeCl_2.4H_2O$ salts precursor registered strong endothermic peak at 400^0C. This indicates that beyond 450^0C there is no weight loss for the synthesized Fe_3O_4 NPs and the nanoparticle is thermally stable. The temperature beyond which the weight loss is insignificant was used for calcination of the synthesized Fe_3O_4 nanoparticles (Herlekar *et al*., 2015).

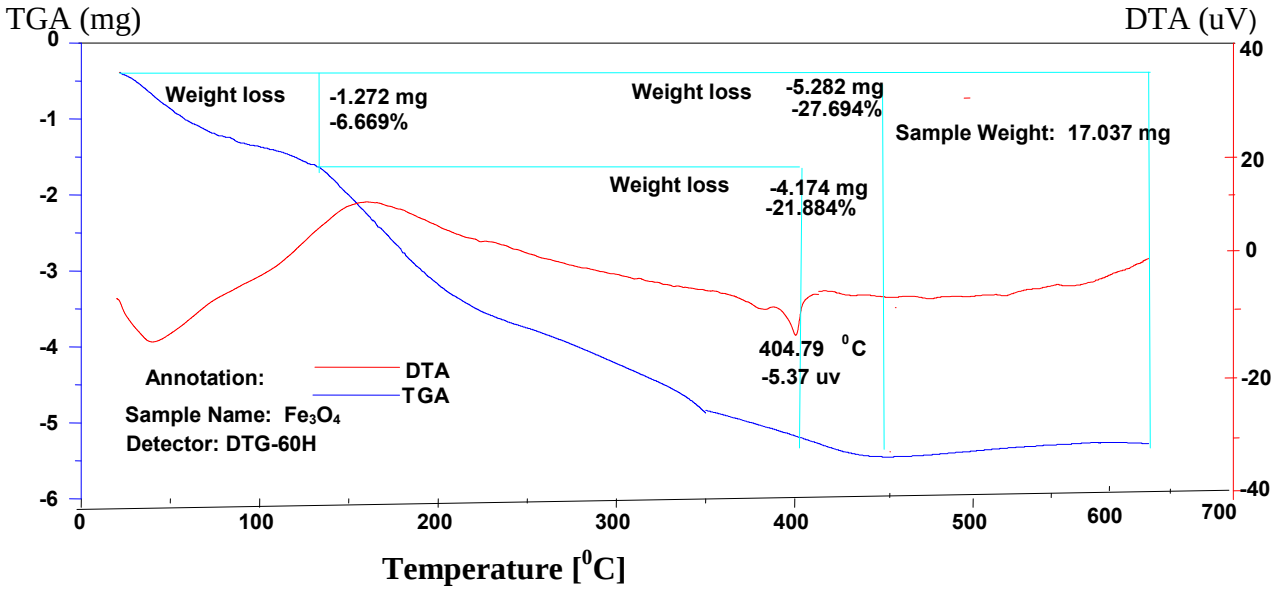

Figure 12: Thermal analysis result for uncalcinated Fe_3O_4 NPs synthesized using ferric chloride hexahydrate, ferrous chloride tetrahydrate precursor and leaf extract of *Thymus schimperi*

4.2 X-Ray Diffraction (XRD) Result

Figure 13 (a, b and c) shows the XRD patterns of Fe_3O_4 NPs synthesized from hexahydrated ferric chloride and tetrahydrated ferrous chloride precursor and *Thymus schimperi* leaf extract.

Fe_3O_4 NPs were synthesized in three ratios by volume of iron salt precursors to *Thymus schimperi* leaf extract. These ratios by volume were designated as S21 for 2:1, S11 for 1:1 and S21 for 1:2 ratios of precursors to plant extract.

The results of peak position (θ), Full Width at Half Maximum (FWHM) of a peak, d-spacing (d-hkl) and Miller indices (hkl) for Fe_3O_4nanoparticles were calculated using an Interactive Powder Diffraction Data Interpretation and indexing program software from XRD data.

As indicated in Figure 13, peaks of Fe_3O_4 NPs synthesized in ratios by volume were observed at 2θ30.15, 31.58, 35.49, 43.12, 45.26, 53.73, 57.11, 62.65^0 for S12; 30.06, 31.67, 35.42, 43.06, 45.38, 53.37, 56.42, 62.55^0 for S11 and at 30.06, 31.56, 35.41, 43.15, 45.25, 53.38, 56.83, 62.56^0 for S21. All the sites and intensity of the diffraction peaks observed were consistent with the standard pattern for JCPDS Card No.79-0417JCPDS for Fe_3O_4nanoparticles synthesis (Ghandoor *et al*., 2012). The broad peaks observed from XRD spectra (Figure 13) indicates that the Fe_3O_4 NPs synthesized were in ultra-fine nature and possess nanoscalecrystallite size (Nishigandh *et al.*, 2015). The observed miller indices for each ratios by volume were (220), (200), (311), (400), (220), (422), (511) and (440) cubic unit cell, which corresponds to cubic spinel structure (Sanpo *et al*., 2013).

The average crystalline size calculated using Debye-Scherer equation (Ghandoor *et al*., 2012) of the diffraction peaks of Fe_3O_4 NPs for these three ratios by volume were found to be 20.26 nm, 29.12 nm and 26.88 nm for S12, S11, and S21, respectively. Even though the three F_3O_4 NPs of different proportions were prepared by the same procedure, there is a slight shift of 2θ position for certain peaks. This might be due to the different ratios of precursors and extracts used that might result in nanoparticles with different sizes, shapes and morphologies. The decreasing in intensity or shifting the peak suggested that interaction of biomolecules present in both precursor and plant leaf extract (Saif *et al*., 2016).

All diffraction peaks of Fe_3O_4 NPs synthesized correspond to the characteristic face centered cubic structure of Fe_3O_4 nanoparticles by comparison with the data from JCPDS Card No.79-0417JCPDS with lattice parameters; a = b = c = 8.39 Å (Ghandoor *et al*., 2012), and the calculated lattice parameters for Fe_3O_4 NPs were 8.38Å, 8.39Å, 8.40Å for S12, S11, S21 respectively. In Table 1 the values of lattice parameter "a" at sharp diffraction peak (d_{311}) for S12 and S21 were estimated which can be attributed to simultaneous formation of another phases such asγ-Fe_2O_3 and α-Fe_2O_3(a = 8.38 and d_{311} = 2.517 for γ-Fe_2O_3 and a = 8.41 and d_{311} = 2.53for α-Fe_2O_3), (Victoria *et al*., 2007). Table 2 shows the lattice parameter of S11 which is in good agreement with the standard data JCPDS: 19-0629 (a = 8.39 Å) (Chaki *et al*., 2015).

Interplanar spacing, at d_{331}, lattice parameter, "a" and crystallite size estimated from XRD(nm) of Fe_3O_4 NPs synthesized using *Thymus schimperi* extract and $FeCl_3.6H_2O$ and $FeCl_2.4H_2O$ for S12, S11 and S21 were shown in Table 3.

The XRD pattern of Fe_3O_4 nanoparticles observed (Figure 14) using salt solution precursor to plant extract in 1:1 ratio (S11) was studied and the sharp intense peak obtained at 2θ of 30.06, 31.67, 35.42, 43.06, 45.38, 53.37, 56.42, 62.55^0 (Table 2) corresponds to the lattice plane (220), (200), (311), (400), (220), (422), (511) and (440), respectively. All the diffraction peaks were well indexed to the hexagonal phase. Figure 14 shows the XRD pattern and crystallographic planes proving the structure of Fe_3O_4 nanoparticles synthesized to be cubic structure (Ref. No. 01-075-0449).

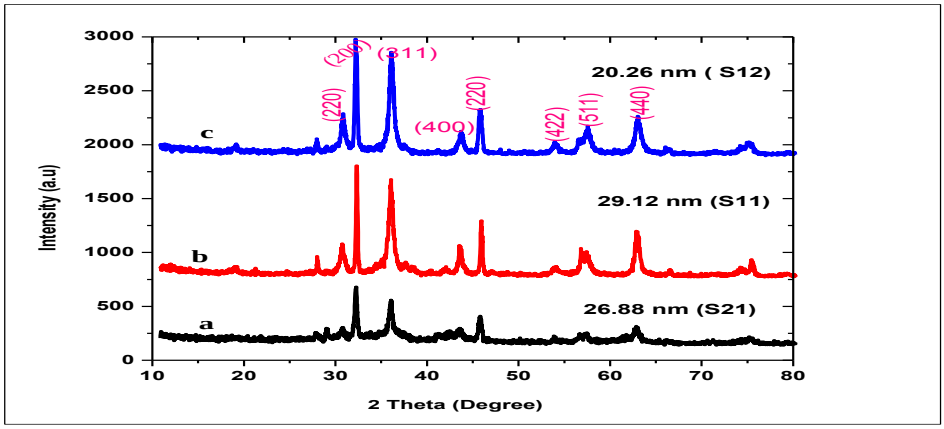

Figure 13: XRD pattern of synthesized Fe3O4 NPs (a) S21, (b) S11 and (c) S12 from $FeCl_3.6H_2O$ and $FeCl_2.4H_2O$ precursor solution and *Thymus schimperi* leaf extract.

According to the Debye-Scherrer formula, the crystallite size D for magnetite iron oxide (Fe_3O_4) nanoparticlesis given by (Ghandoor *et al*. 2012):

$$D = \frac{0.94\ \lambda}{\beta cos\theta} \tag{4.1}$$

Where, D is the Crystallite size, λ is the X-ray wavelength (1.5406 Å), β is the Full Width at Half Maximum (FWHM) of a peak, and θ is the peak position.

The lattice parameter "a_o" of Fe_3O_4 nanoparticles from XRD result is determined by (Chaki *et al*., 2015):

$$d_{hkl} = \frac{a}{\sqrt{h^2 + k^2 + l^2}} \tag{4.2}$$

Table 1 shows different angles, interplanar spaces (d-hkl), FWHM values, lattice planes (hkl), lattice parameter and sizes of Fe_3O_4 NPs for S21 and S12 synthesized using *Thymus schimperi* leaf extract and $FeCl_3.6H_2O$ and $FeCl_2.4H_2O$ solution.

Table 1: Different angles, interplanar spaces (d-hkl), FWHM values, lattice plane, lattice parameter and sizes of Fe_3O_4 nanoparticles for S21 and S12

Fe_3O_4 NPs (S12)						Fe_3O_4 NPs (S21)					
2θ	(d-hkl)	FWHM	(hkl)	"a" (Å)	size (nm)	2θ	(d-hkl)	FWHM	(hkl)	"a" (Å)	size (nm)
30.15	2.9619	0.4700	220	8.37	18.0	30.06	2.9706	0.3300	220	8.40	25.3
31.58	2.8306	0.3377	200	5.66	25.3	31.56	2.8322	0.3140	200	5.66	27.3
35.49	2.5273	0.5612	311	8.38	15.5	35.41	2.5329	0.4244	311	8.40	20.6
43.12	2.0961	0.5400	400	8.37	16.6	43.15	2.0947	0.3734	400	8.37	23.7
45.26	2.0019	0.4279	220	5.66	20.9	45.25	2.0025	0.3900	220	5.66	22.9
53.73	1.7047	0.3200	311	8.35	28.9	53.38	1.7151	0.2600	422	8.40	34.4
57.11	1.6116	0.4266	511	8.37	22.2	56.83	1.6189	0.3400	511	8.41	27.3
62.65	1.4816	0.6633	440	8.38	14.7	62.56	1.4835	0.2880	44 0	8.39	33.6
Average crystallite size **20.26**						Average crystallite size **26.88**					

Table 2 shows different angles, interplanar spaces (d-hkl), FWHM values, lattice planes (hkl), lattice parameter and sizes of Fe_3O_4 NPs for S11 synthesized using *Thymus schimperi* leaf extract and $FeCl_3.6H_2O$ and $FeCl_2.4H_2O$ solution.

Table 2: Different angles, interplanar spaces (d-hkl), FWHM values, lattice plane, lattice parameter and sizes of Fe_3O_4 nanoparticles for S11

Fe_3O_4 NPs (S11)					
2θ (degree)	Interplanar spacing (d-hkl) (Å)	FWHM (degree)	Lattice plane (hkl)	Lattice parameter "a" (Å)	Size of Fe_3O_4 NPs
30.06	2.9701	0.5400	220	8.40	15.7
31.67	2.8233	0.1917	200	5.64	42.5
35.42	2.5324	0.5258	311	8.39	16.4
43.06	2.0988	0.3573	400	8.39	24.5
45.38	1.9968	0.2124	220	5.64	41.3
53.37	1.7154	0.2800	422	8.40	32.9
56.42	1.6297	0.2400	511	8.46	39.1
62.5	1.4839	0.4611	440	8.39	20.6
Average crystallite size **29.12**					

Table 3 shows Interplanar spacing, at d_{331}, lattice parameter, "a" and crystallite size estimated from XRD (nm) of Fe_3O_4 NPs synthesized using *Thymus schimperi* extract and $FeCl_3.6H_2O$ and $FeCl_2.4H_2O$ for S12, S11 and S21.

Table 3: Interplanar spacing at d_{331}, lattice parameter and Crystallite size estimated from XRD (nm) of S12, S11 and S21

Sample	Interplanar spacing d_{311}(Å)	Lattice parameter "a" (Å)	Crystallite size estimated from XRD(nm)
S21	2.5329	8.40	20.6
S11	2.5324	8.39	16.4
S12	2.5273	8.38	15.5

The XRD pattern of Fe_3O_4 synthesized nanoparticles using $FeCl_3.6H_2O$ and $FeCl_2.4H_2O$ precursor and *Thymus schimperi* leaf extract in 1:1 ratio (S11) was studied and the sharp intense peaks obtained at 2**θ**30.06, 31.67, 35.42, 43.06, 45.38, 53.37, 56.42 and 62.55 corresponds to the lattice plane (220), (200), (311), (400), (220), (422), (511) and (440), respectively.

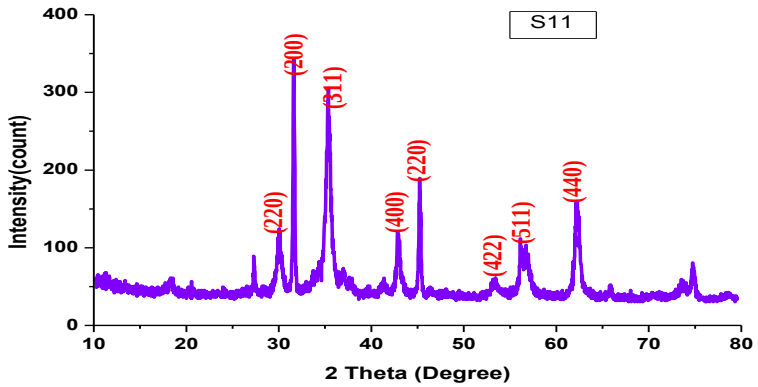

Figure 14: XRD pattern and labeled lattice plane of S11

4.3 Fourier Transformed Infrared (FT-IR) Analysis Result

This FT-IR gives information on the vibration and rotational modes of motion of a molecule and hence an important technique for identification and characterization of a substance. The Infrared spectrum of an organic compound provides a unique fingerprint, which is readily distinguished from the absorption patterns of all other compounds; only optical isomers absorb in exactly the same way. Hence FT-IR is an important technique for identification and characterization of a substance (Smith *et al*., 1998).

The vibrational phenomenon and the quality of Fe_3O_4 NPs were characterized by Fourier Transformed Infrared (FT-IR) in the wave number range of 400-4000 cm^{-1}. Fourier transform infra-red (FTIR) spectra of magnetite nanoparticles synthesized using *Thymus schimper* leaf extracts was shown in Figure 15. Measurements of were performed by putting the powder of Fe_3O_4 NPs on KBr plate.

Figure 15(a) shows the FT-IR spectra of calcinated green synthesized Fe_3O_4 NPs which revealed strong absorption bands at 3440, 1622, 1425, 875 and 570 cm^{-1}while Figure 15(b) shows the absorption bands of uncalcinated synthesized Fe_3O_4 NPs were observed at 3420, 2959, 1623, 1456, 1377, 1064 and 600cm^{-1}.

In the calcinated Fe_3O_4 NPs spectrum, the wide absorption around 3440 cm^{-1} is caused by the presence of an O-H stretching vibrations due to the absorbed water on the surface of the samples. The absorption peaks at 1622 cm^{-1} were attributed to the N-H bending of amide compound.1425cm^{-1} corresponded to the -CH_2 bending vibrations of the compound. Significant new peak was found at 875 cm^{-1} which indicates C-H bending and the band at 570 cm^{-1} indicated the Fe-O stretching of Fe_3O_4 nanoparticles, as reported earlier (Gotic *et al.,* 2009) which indicated the formation of Fe_3O_4 nanoparticles.

Figure 15 (b) shows the FT-IR spectra of uncalcinated synthesized Fe_3O_4 NPs and the wide absorption around 3420 cm^{-1} is caused by the presence of an O-H stretching vibrations due to the absorbed water on the surface of the samples. The absorption peaks at 2959 cm^{-1} and 1456 cm^{-1} were also attributed to the -CH_2 stretching vibrations of the functional group (Awwad *et al*., 2012). 1623 cm^{-1} corresponded to the N-H bending vibrations of the compound and 1377 cm^{-1} to bending functional group of the O-H. The peaks at 1051 cm^{-1} revealed C-N bond and 600 cm^{-1} indicates C-O stretching band related to the C-O-SO_3 group (Camara *et al*., 2011).

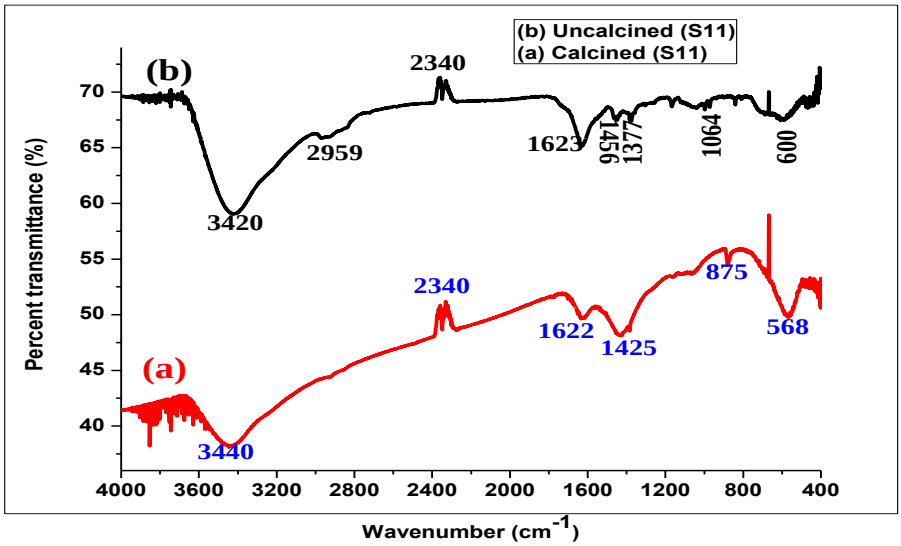

Figure 15: FT-IR spectrum (a) for calcinated, (b) for uncalcinated Fe_3O_4 NPs synthesized using hexahydrated ferric chloride and tetra hydrated ferrous chloride precursor and *Thymus schimperi* leaf extract.

4.4 Scanning Electron Microscope (SEM) Analysis Result

The morphology of Fe_3O_4 nanoparticles were studied using SEM images. The surface morphology of the synthesized samples was viewed through the high resolution scanning electron microscope. SEM images of Fe_3O_4 NPs have different morphology as shown in Figure 16 (a-d). The morphology of uncalcined Fe_3O_4 NPs as indicated in Figure 16 (a) is not clearly identified. The SEM images of calcined Fe_3O_4 NPs in Figure 16 (b-d) indicate the agglomeration of particles that increases with the concentration of iron salts precursor. The morphology of Fe_3O_4 NPs synthesized from mixture of hydrtaed ferric and ferrous chloride in different mixing ratio of precursor to extract such as 2:1, 1:1 and 1:2 have agglomerated cubic spinel structure. The scanning electron microscope results confirmed that the grain sizes of the synthesized NPs were strongly dependent on mixing ratio of iron salts & leave extracts under the same reaction conditions.

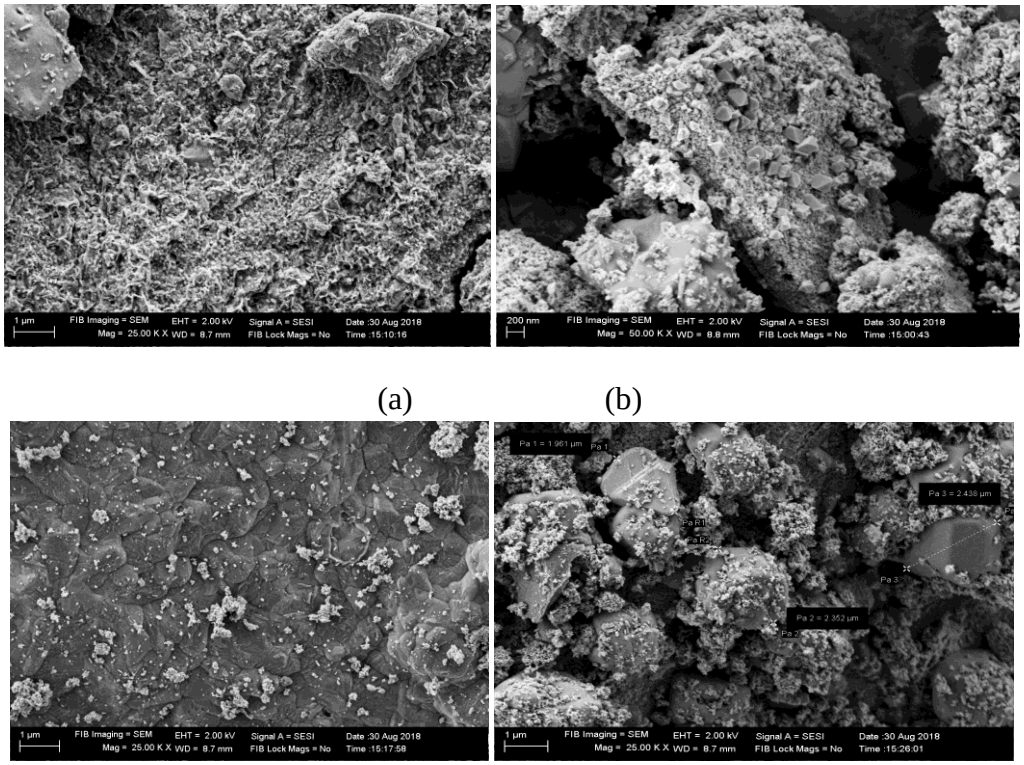

Figure 16: SEM images of Fe_3O_4 NPs synthesized using precursor to extract: (a) for uncalcined in (1:1), (b) for calcined S11 in (1:1), (c) for calcined S12 in (1:2) and (d) for calcined S21 in (2:1).

The SEM image results also agreed with XRD results obtained, i.e. the crystal sizes in XRD with big size have also big shapes in SEM images. This indicates that Fe_3O_4 NPs have successfully prepared using iron salts precursor to extract within a nano range. The SEM images clearly show micro structural homogeneities and remarkably different morphology for Fe_3O_4 powder.

4.5 Energy Dispersive X-Ray Spectroscopy (EDX) Analysis Result

The composition of the samples was determined by energy dispersive X-Ray spectroscopy (EDX) using scanning microscope. The energy dispersive X-ray analyses of all Fe_3O_4 NPs were shown in Figures 17(a-h). It is evident from the X-ray patterns of all the samples in which Fe and O are found in the respective spectrum. In addition to that interestingly it is observed there were foreign material present in the spectrum. It is added confirmation for the impurity of the samples.

Quantitative analyses of the samples were indicated in the Tables 4-7. All tables also shows impurities are found out.

ZAF in Table refers to matrix correction:
Z = Atomic number correction,
A = Absorption correction, F = Fluorescence correction.

Table 4: Quantitative analysis of uncalied S11 (1:1)

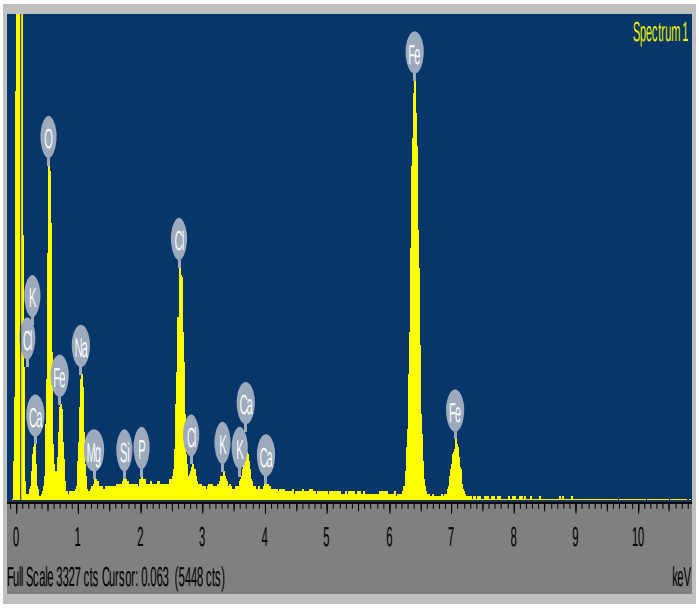

Element	Weight%	Atomic%
O K	29.74	53.41
Na K	9.37	11.71
Mg K	0.65	0.76
Si K	0.21	0.21
P K	0.24	0.22
Cl K	8.27	6.70
K K	0.56	0.41
Ca K	1.70	1.22
Fe K	49.27	25.35
Matrix	**Correction**	**ZAF**

Figure 17(a): EDX spectrum of uncalcined S11

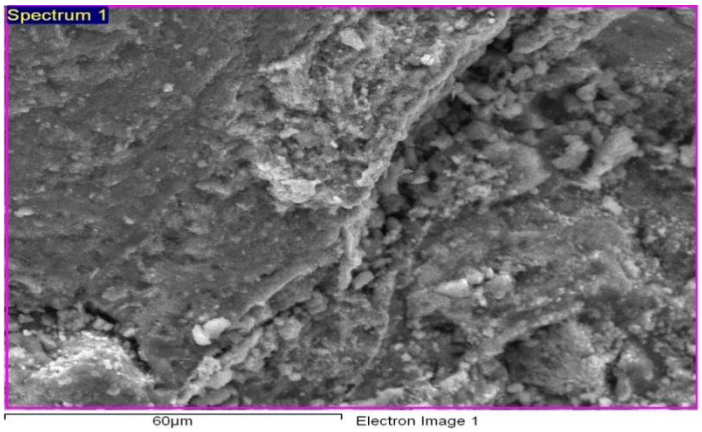

The weight % for iron and oxygen were 49.27% and 29.74%respectively giving a total of 79.01% and also the atomic % were 25.35% and 53.41% respectively giving a total of 78.76%. The total weight % and atomic % for other components were 20.99% and 21.24respectively.

Figure 17(b): SEM images of selected EDX spectra for uncalcined S11

Table 5: Quantitative analysis of calcined S11

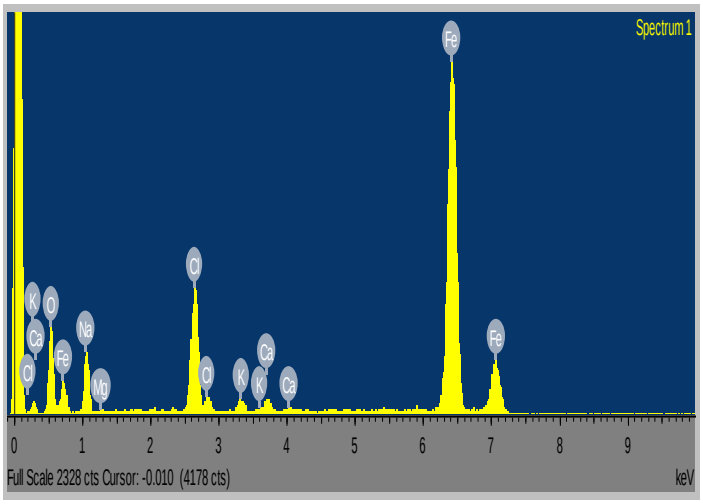

Element	Weight%	Atomic%
O K	13.25	30.49
Na K	9.02	14.44
Mg K	0.33	0.50
Cl K	8.10	8.41
K K	0.90	0.85
Ca K	0.84	0.77
Fe K	67.56	44.54
Matrix	**Correction**	**ZAF**

Figure 17(c): EDX spectrum of calcined S11

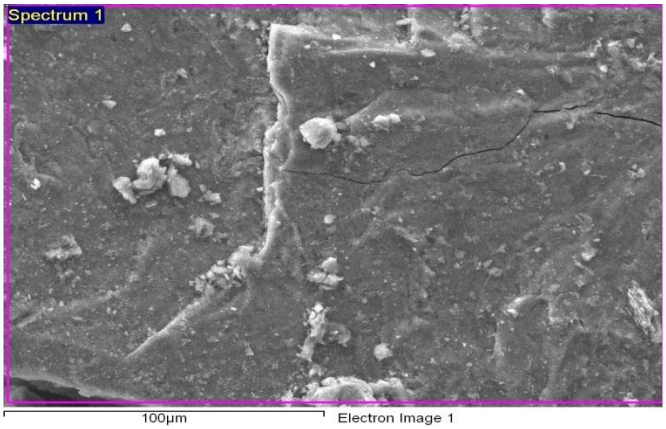

The weight % for iron and oxygen were 67.56% and 13.25%respectively giving a total of 80.81% and also the atomic % were 44.54% and 30.49% respectively giving a total of 75.03%. The total weight % and atomic % for other components were 19.19% and 24.97respectively.

Figure 17(d): SEM images of selected EDX spectra for calcined S11

Table 6: Quantitative analysis of calcined S12

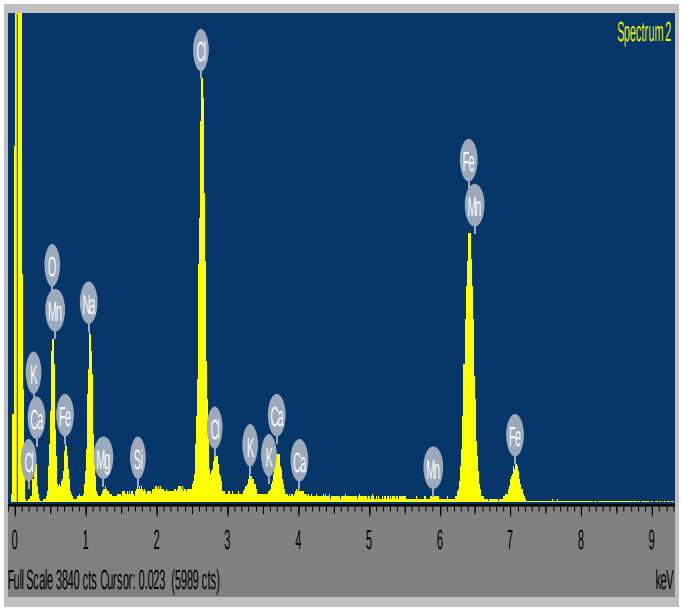

Element	Weight%	Atomic%
O K	23.57	42.92
Na K	13.93	17.65
Mg K	0.52	0.63
Si K	0.30	0.31
Cl K	18.62	15.30
K K	1.03	0.77
Ca K	2.46	1.79
Mn K	0.37	0.19
Fe K	39.20	20.44
Matrix	**Correction**	**ZAF**

Figure 17(e): EDX spectrum of calcined S12

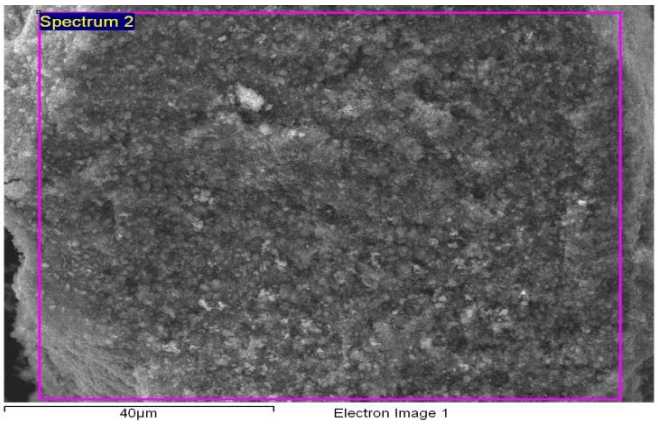

The weight % for iron and oxygen were 39.20% and 23.57%respectively giving a total of 62.77% and also the atomic % were 20.44% and 42.92% respectively giving a total of 63.36%. The total weight % and atomic % for other components were 37.23% and 36.64respectively.

Figure 17(f): SEM images of selected EDX spectra for calcined S12

Table 7: Quantitative analysis of calcined S21

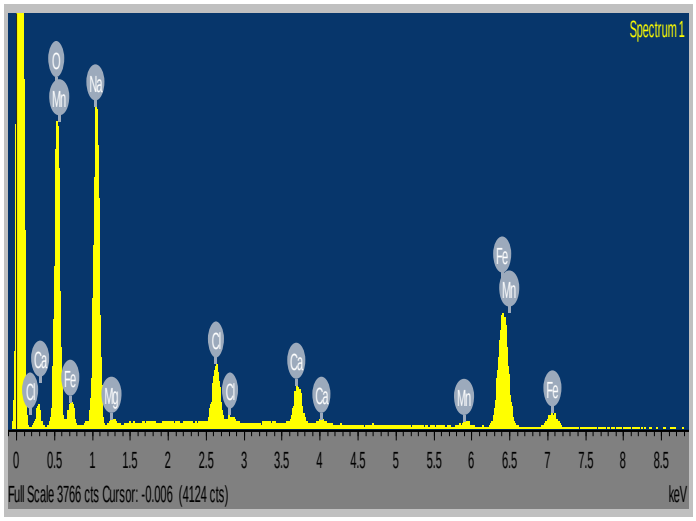

Element	Weight%	Atomic%
O K	39.21	56.03
Na K	29.78	29.61
Mg K	0.64	0.60
Cl K	3.67	2.37
Ca K	2.87	1.64
Mn K	0.81	0.34
Fe K	23.01	9.42
Matrix	**Correction**	**ZAF**

Figure 17(g): EDX spectrum of calcined S21

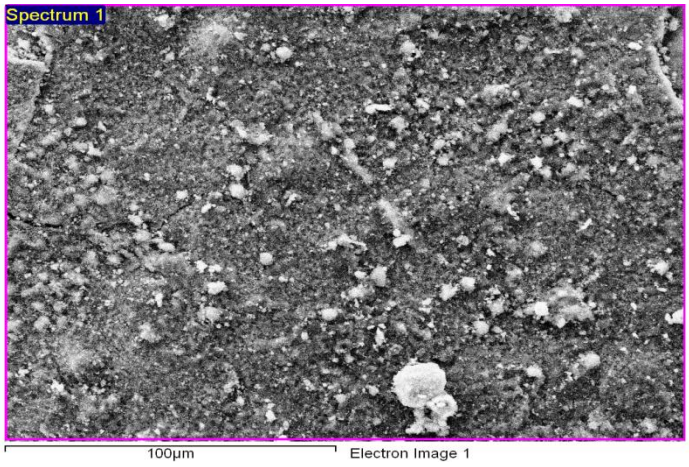

The weight % for iron and oxygen were 23.01% and 39.21%respectively giving a total of 62.22% and also the atomic % were 9.42% and 56.03% respectively giving a total of 65.45%. The total weight % and atomic % for other components were 37.78% and 34.55respectively.

Figure 17(h): SEM images of selected EDX spectra for calcined S21

The EDX spectrum (Figure 17 a, c, e and g) shows that all samples of Fe_3O_4 NPs were synthesized and the signals of iron and oxygen have been detected, suggesting that the nanoparticle is made up of Fe and O and have some amounts other compositions. The energy dispersive spectra of the samples obtained from the SEM-EDX analysis (Figure 17 c and d) clearly show that the sample prepared by the above route has higher purityof Fe and O than other phases.

4.6 UV-Vis spectroscopy Analysis Result

The UV-Vis reflectance spectra of uncalcined and calcinated Fe_3O_4 NPs prepared were shown in Figure 18. The reflectance peak of the Fe3O4 NPs prepared for uncalcinated was found at around 325 nm and for calcinated Fe_3O_4 NPs for S11, S12 and S21 was found in between 321-324 nm. As seen in Figures, the reflection peak in between 320-350 nm may be due to the oxidation of zero valent iron to iron oxide nanoparticles (Guo *et al*., 2001).

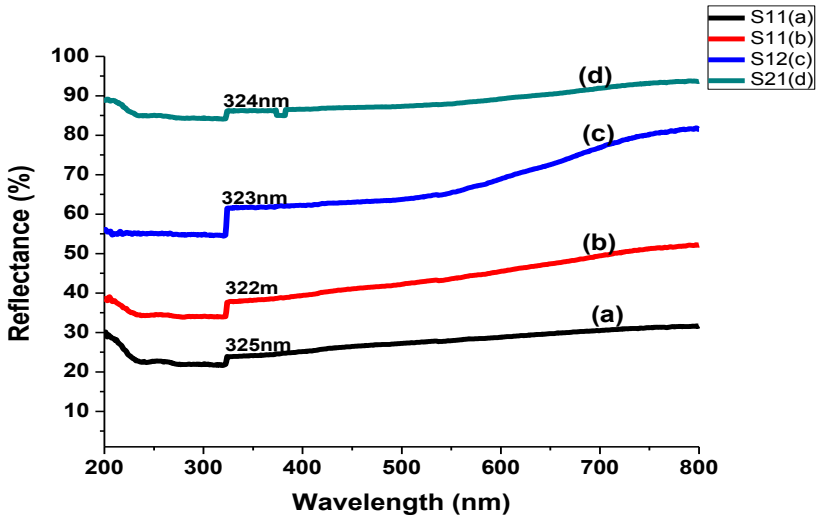

Figure 18: Uv-Vis reflectance spectra of uncalcinated (a) S11 and calcinated (b) S11, (c) S12 and (d) S21 Fe_3O_4 NPs.

4.7 Application of Fe_3O_4 NPs for Cr(VI) and Hg(II) Removal

The calibration curve before Cr(VI) and Hg(II) removal was drawn (appendix 3 and 4) by measuring the absorbance of different known concentrations of chromium and mercury solutions and then graph between concentrations versus absorbance was plotted. From the plotted standard curves, the slope of two solutions were $y = 0.005x + 1.865$ with $R^2 = 0.992$ for chromium solution (appendix 3) and $y=0.002x + 0.190$ with $R^2= 0.997$ for mercury solution (appendix 4) respectively.

4.7.1 Optimization of Different Parameters

The optimization processes of variables were done to get maximum % removal of chromium and mercury. At initial concentration of 20mg/L, maximum removal of 85% chromium and 95% of mercury was achieved with the magnetite (Fe_3O_4) nanoparticles by keeping other parameters constant (pH = 3, contact time = 90min, adsorbent dosage = 300mg). At pH 5, 84% chromium and at pH 7, 85% of mercury removal was achieved (C*o*=20mg/L, contact time = 90min, adsorbent dosage= 300mg). 84% of chromium and 90% of mercury was removed at adsorbent dosage 700mg (C*o* = 20mg/L, contact time = 90min and pH = 3). Removal efficiency for chromium at 60 min was 86% and at 90 min for mercury was 90% by keeping other parameters constant (pH = 3, C*o* = 20mg/L, absorbent dosage = 300mg).

4.7.2 Factors Affecting the Adsorption

Various factors influence the adsorption capacity of potential adsorbents during the adsorption process. Efficiency of any adsorbent is strongly influenced by the physicochemical characteristics of the solutions such as pH, initial concentration, contact time and adsorbent dosage. Higher adsorption capacities can be obtained by optimizing the above parameters (Hua*et al*., 2012).

4.7.2.1 Effect of initial concentration

Initial concentration of metal ions can alter the metal removal efficiency through a combination of factors such as the availability of specific surface functional groups and the ability of surface functional groups to bind metal ions. Initial concentration of solution can provide an important driving force to overcome the mass transfer resistance of metal between the aqueous and solid phases (Adegoke *et al*., 2013).

The initial concentration of chromium and mercury ions were varied from 20 mg/L to 80 mg/L, by keeping other parameters constant (pH=3,contacttime = 90min, absorbent dosage=300mg). The equilibrium curve shows that the overall percent removal for both Cr(VI) and Hg(II) from solution decreases with an increase in initial of concentration Cr(VI) and Hg(II). This may be attributed to the fact that with increase in concentration/amount of Cr(VI) or Hg(II) in solution with fixed amount of adsorbent, binding capacity of adsorbent approaches to saturation resulting in decrease in both Cr(VI) and Hg(II) removal. At higher Cr(VI) and Hg(II) concentration; the number of active sites on adsorbent surface is not enough to accommodate both chromium and mercury ions, however, at low concentration, the ratio of surface active sites to total concentration of Cr (VI) and Hg(II) were high and therefore the two of metal ions can interact with the active sites on adsorbent surface sufficiently.

Figure 19 shows effect of initial concentration of aqueous solution on removal efficiency of biosynthesized Fe_3O_4 NPs using *Thymus schimperi*.

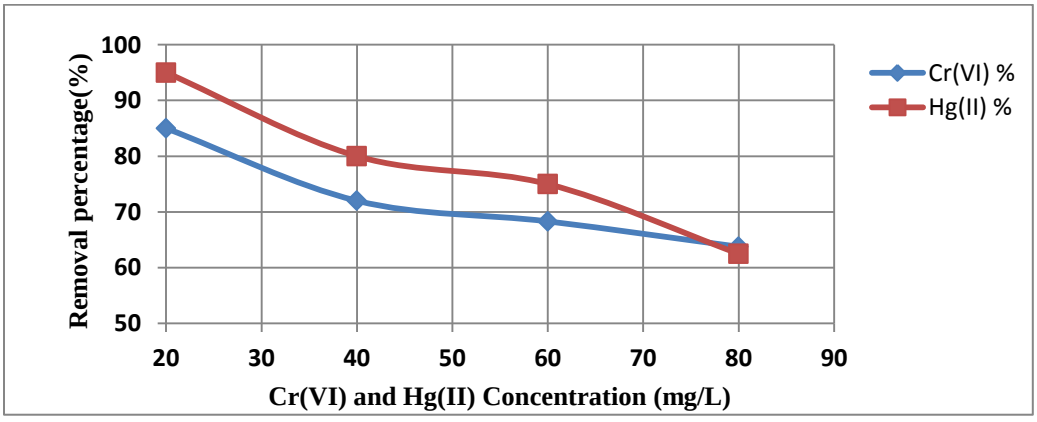

Figure 19: Influence of initial concentration of Cr(VI) and Hg(II) ions on removal efficiency of biosynthesized Fe_3O_4 NPs using *Thymus schimperi*.

4.7.2.2 Effect of pH on adsorption

The pH of a solution is a significant parameter in the adsorption process. It affects both the dissociation degree of the functional groups from the adsorbent surface and the solubility of the metal ions. Thus, experiments were performed in order to investigate the effect of initial pH of solution to be treated. Different species of Hg(II) and Cr(VI) are greatly dependent on pH of the solution (Denizli *et al*., 2003; Ansari *et al*., 2007), and the pH values selected in this experiments were 3-11.During this study, results showed that the removal of metal ions was strongly dependent on the pH of the solution. Chromium and mercury removal by Fe_3O_4 NPs sorbent increased varying pH from 3 to 5 for chromium and 3 to 7 for mercury. It must be emphasized that up to pH 7.0 no mercury and up to pH 5 no chromium precipitation occurred, and the concentrations of Hg(II) and Cr(VI) were almost unchanged when altering pH without the adsorbent.

Figure 20 shows the effect of pH on removal efficiency of biosynthesized Fe_3O_4 NPs using *Thymus schimperi* on Cr(VI) and Hg(II) from aqueous solution.

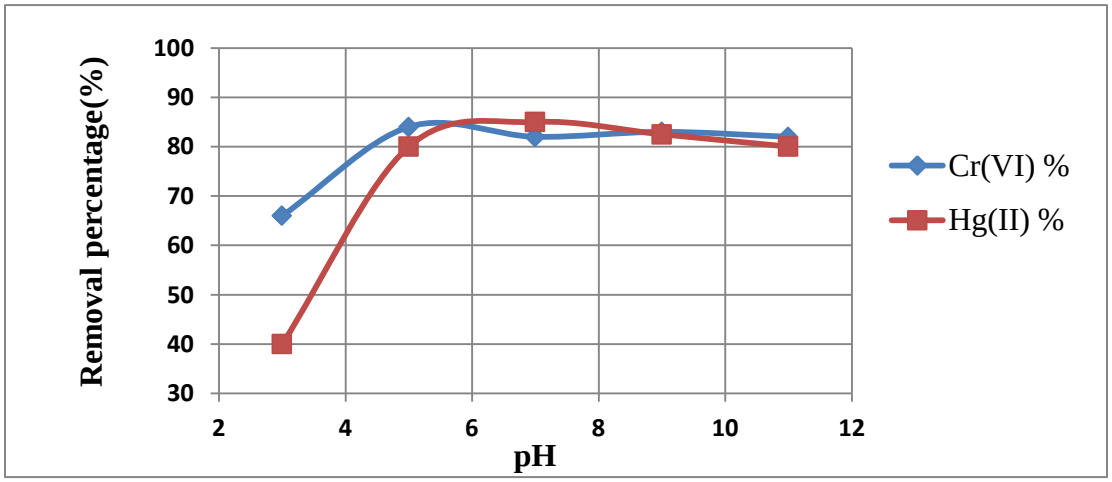

Figure 20: Effect of pH on removal efficiency of biosynthesized Fe_3O_4 NPs using *Thymus schimperi* on Cr(VI) and Hg(II)from aqueous solution.

4.7.2.3 Effect of contact time

Contact time is necessarily a fundamental parameter in adsorption. Therefore, it is important to study its effect on the sorption capacity of the magnetic sorbent. Adsorptions can be assumed to be complete when equilibrium is achieved between the solute of solution and the adsorbent. However, specific time is needed to maintain the equilibrium interactions to ensure that the adsorption process is complete.

The adsorption experiments were carried out for different contact times with fixed sorbent dose, pH, and initial concentration. The results were plotted in Figure 21, as it is shown, the removal efficiency of chromium and mercury by the adsorbent significantly increase during the initial adsorption stage and then continue to increase at a relatively slow speed with contact time until a state of equilibrium is attained. Generally, the removal rate of sorbate is rapid initially, but it gradually decreases with time until it reaches equilibrium.

This phenomenon can be attributed to the fact that a large number of vacant surface sites are available for adsorption at the initial stage, and after a lapse of time, the remaining vacant surface sites are difficult to be occupied due to repulsive forces between the solute molecules on the solid and bulk phases.

Figure 21 shows effect of contact time on removal efficiency of biosynthesized Fe_3O_4 NPs using *Thymus schimperi* on Cr(VI) and Hg(II) from aqueous solution.

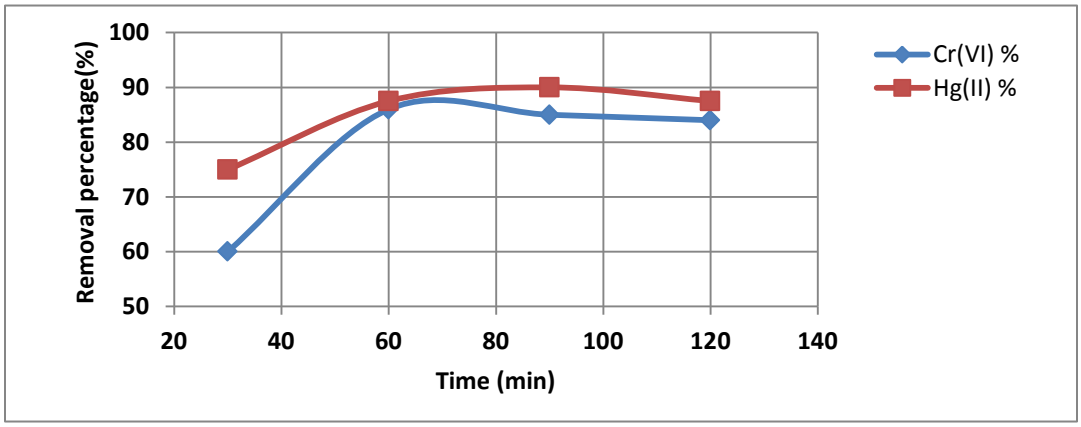

Figure 21: Effect of contact time on removal efficiency of biosynthesized Fe_3O_4 NPs using *Thymus schimperi* on Cr(VI) and Hg(II) from aqueous solution.

4.7.2.4 Effect of adsorbent dosage

Adsorbent dose seems to have a great influence on adsorption process. Figure 22 shows that removal increased with increasing the amount of adsorbent dosage. These results indicate that removal efficiency is directly related to the number of available adsorption sites. This suggests that after a certain dose of adsorbent, the maximum adsorption sets in and hence the amount of ions bound to the adsorbent and the amount of free ions remains constant even with further addition of the dose of adsorbent. Amount of adsorbent added to the solution determines the number of binding sites available for adsorption. Metals adsorption efficiency was increased with increase in adsorbent dose. This revealed that the adsorption sites remain unsaturated during the adsorption reaction whereas the number of sites available for adsorption site increases by increasing the adsorbent dose.

Figure 22 shows effect of adsorbent dose on removal efficiency of biosynthesized Fe_3O_4 NPs using *Thymus schimperi* on Cr(VI) and Hg(II) from aqueous solution.

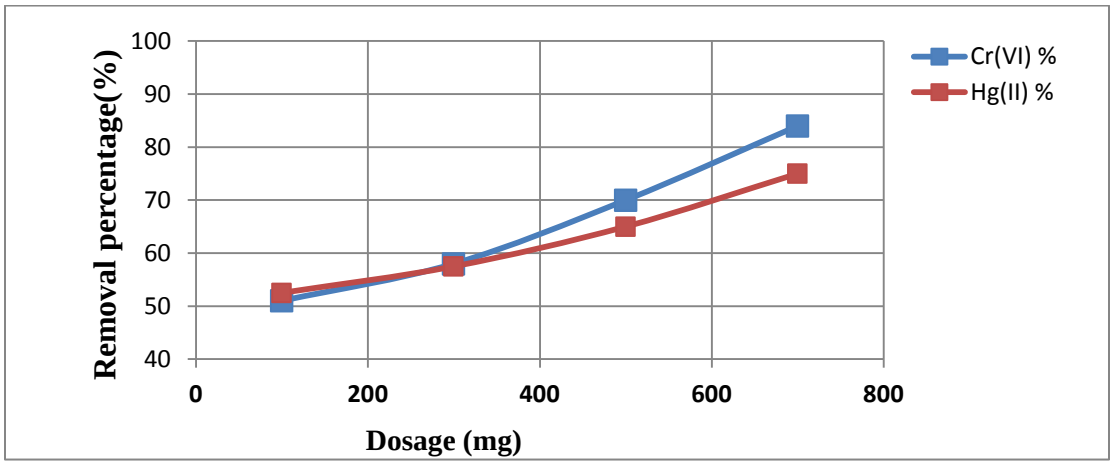

Figure 22: Influence of amount of synthesized Fe_3O_4 NPs sorbent using *Thymus schimperi* on Cr(VI) and Hg(II) from aqueous solution.

4.8 Sorption kinetics

Equilibrium study is vital in determining the efficacy of adsorption. It is also necessary to identify the adsorption mechanism for a given system. Kinetic models have been exploited to test the experimental data and to find the mechanism of adsorption and its potential rate-controlling step that include mass transport and chemical reaction. In addition, information on the kinetics of metal uptake is required to select the optimum conditions for full scale batch or continuous metal removal processes. Adsorption kinetics is expressed as the solute removal rate that controls the residence time of the sorbate in the solid-solution interface. Several kinetic models are used to explain the mechanism of adsorption processes. These models include Pseudo-first-order rate model and Pseudo-second order rate model.

In order to define the adsorption kinetics of heavy metal ions, the kinetics parameters for the adsorption process were studied for contact times ranging from 1 to 120 min by monitoring the removal percentage of the Cr (VI) and Hg (II).

4.8.1 Pseudo first order model

The Pseudo first order rate model based on adsorption capacity of adsorbent and is generally expressed as:

$$\log(Q_e - Q_t) = \log Q_e - k_1 t \qquad (4.3)$$

Where, *Qe* and *Qt* are the amounts (mg/g) of Cr (VI) and Hg(II) adsorbed at equilibrium and at time (t), respectively. Plot of log (*Qe* - *Qt*) versus t gives a straight line for first order adsorption kinetics which allows computation of the rate constant k_1.

Figure 23 shows Pseudo first order kinetics model for biosynthesized Fe_3O_4 NPs using *Thymus schimperi* on Cr(VI) and Hg(II) from aqueous solution.

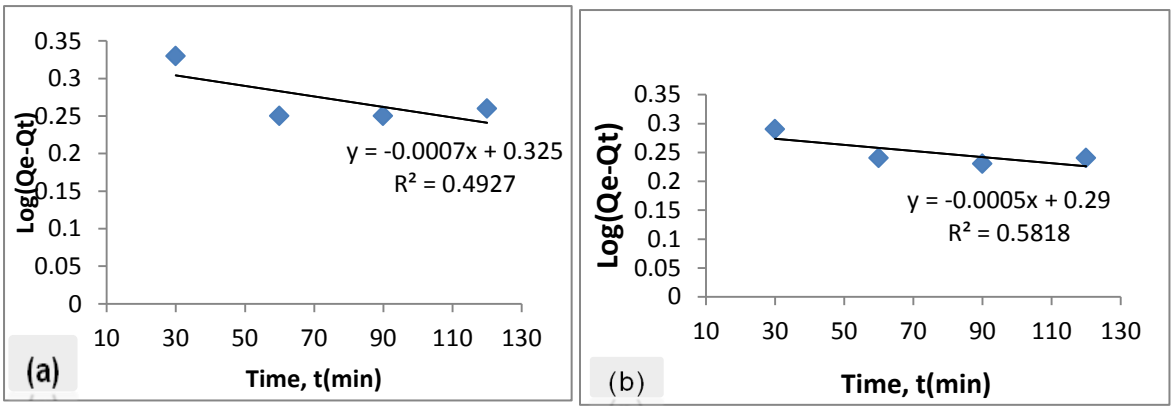

Figure 23: Pseudo first order kinetic model for biosynthesized Fe_3O_4 NPs using *Thymus schimperi* on Cr(VI) and Hg(II) from aqueous solution.

4.8.2 Pseudo-second order model

The equation that describes the pseudo-second order model is given in the following linear form

$$\frac{t}{q_t} = \frac{1}{k_2 q_e^2} + \frac{1}{q_e} t \qquad (4.4)$$

Where k_2 is the adsorption rate constant (g/mg-min). The k_2 and q_e are found from the intercept and slop of t/q_t versus t linear plot such that q_e = 1/slope and k_2 = slope^2/intercept.

Figure 24 shows Pseudo second order kinetics model for biosynthesized Fe_3O_4 NPs using *Thymus schimperi* on Cr(VI) and Hg(II) from aqueous solution.

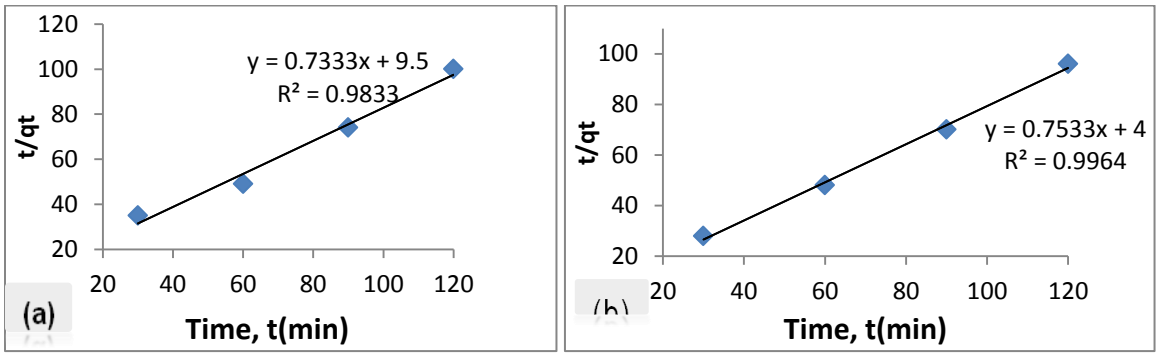

Figure 24: Pseudo second order kinetics model for biosynthesized Fe_3O_4 NPs using *Thymus schimperi* on Cr(VI) and Hg(II) from aqueous solution.

The degree of goodness of linear plot of these kinetic models can be judged from the value of the determination coefficient of the plot, which can also be regarded as a criterion in the determination of the adequacy of kinetic model. The kinetic rate constants obtained from pseudo-first order and pseudo-second-order models are given in Table 8. Pseudo-second order kinetics present high correlation coefficients than pseudo-first-order and the experimental qe values obtained are closer to those calculated for the pseudo-second order kinetic model. External mass transfer and intraparticle diffusion represent the experimental kinetics where the effect of pore diffusion and film diffusion are expected to negligible respectively.

Table 8 shows the summary of pseudo first and second order kinetics fit parameter for synthesized Fe_3O_4 NPs using *Thymus schimperi* on removal of Cr(VI) and Hg(II) from aqueous solution.

Table 8: The adsorption kinetic model rate constants for adsorption of chromium and mercury

Metal ions	Pseudo 1st order kinetic model			Pseudo 2nd order kinetic model		
	q_e	K_1	R^2	q_e	K_2	R^2
Cr(VI)	2.11	0.00	0.492	1.36	0.057	0.983
Hg(II)	1.95	0.00	0.581	1.33	0.142	0.996

4.9 Sorption isotherm

The adsorption isotherm is fundamental in describing the interactive behavior between solutes and adsorbent, which express the surface properties and affinity of the adsorbent. It also plays an important role in the design of an adsorption system. The Langmuir and Freundlich models are often used to describe equilibrium adsorption isotherms.

4.9.1 Langmuir isotherm

The Langmuir isotherm assumes monolayer adsorption onto a surface containing a finite number of adsorption sites of uniform strategies with no transmigration of adsorbate in the plane surface. Once a site is filled, no further sorption can take place at that site. This indicates that the surface reaches a saturation point where the maximum adsorption of the surface will be achieved. The isotherm is represented by

$$\frac{C_e}{q_e} = \frac{K_L C_e}{Q_o} + \frac{1}{Q_o} \tag{4.5}$$

where q_e (mg/g) and C_e (mg/L) are the amount of adsorbed chromium or mercury per unit mass of sorbent and unadsorbed chromium or mercury concentration in solution at equilibrium, respectively. Q_o is the maximum adsorption at monolayer (mg g^{-1}) on the surface bound at high C_e, and K_L is a constant related to the affinity of the binding sites (L/mg).

The Langmuir constants Q_o and K_L were determined from the intercept and slope of the linear plot of (C_e /qe) against the equilibrium concentration (C_e).

The essential features of the Langmuir isotherm may be expressed in terms of equilibrium parameter R_L, which is a dimensionless constant referred to as separation factor or equilibrium parameter.

$$R_L = \frac{1}{1 + K_L C_o} \tag{4.6}$$

Where: C_0 = initial concentration, K_L = the constant related to the energy of adsorption (Langmuir Constant). R_L value indicates the adsorption nature to be either unfavourable if R_L>1), linear if R_L =1, favorable if 0<R_L<1 and irreversible if R_L=0.

From the data calculated, the R_L for Cr(VI)and Hg(II) is greater than 0 but less than 1 indicating that Langmuir isotherm is favorable. From Figure 25 (a), the maximum monolayer coverage capacity (Q_o) from Langmuir Isotherm model for Cr(VI) was determined to be 0.951mg/g, K_L (Langmuir isotherm constant) is 0.078 L/mg, R_L(the separation factor) is 0.391, 0.243, 0.176 and 0.138 for 20, 30, 40 and 80mg/L of initial concentration respectively. This reflects that in all the cases, R_L values fall between 0 and 1, indicating favorable adsorption of Cr (VI) and the R^2 value is 0.93 proving that the sorption data fitted well to Langmuir Isotherm model.

From Figure 25 (b), the maximum monolayer coverage capacity (Q_o) from Langmuir Isotherm model for Hg(II) was determined to be 2.631mg/g, K_L (Langmuir isotherm constant) is 0.287 L/mg, R_L(the separation factor) is 0.148, 0.080, 0.055 and 0.042 for 20, 30, 40 and 80mg/L of initial concentration respectively. This reflects that in all the cases, R_L values fall between 0 and 1, indicating favorable adsorption of Hg (II) and the R^2 value is 0.98 proving that the sorption data fitted well to Langmuir isotherm model.

Figure 25 shows Langmuir isotherm for Cr (VI) and (b) for Hg (II) ion adsorption from aqueous solution using biosynthesized Fe_3O_4 NPs adsorbent.

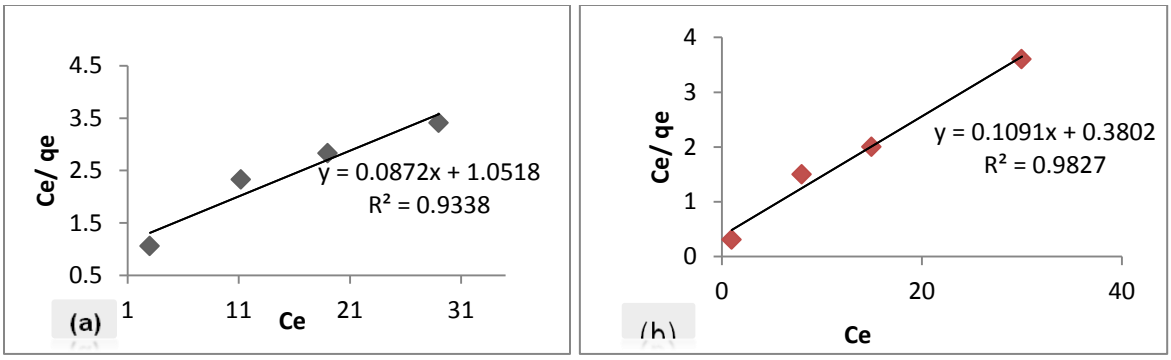

Figure 25: (a) Langmuir isotherm for Cr(VI) and (b) for Hg(II) ion adsorption using synthesized Fe_3O_4 NPs.

4.9.2 Freundlich isotherm

Freundlich isotherm is an empirical equation employed to describe heterogeneous systems. The Freundlich equation is expressed as:

$$q_e = K_f C_e^{1/n} \tag{4.7}$$

Where K_f and n are Freundlich constants with K_f (mg/g (L/mg) $^{1/n}$) is the adsorption capacity of the sorbent and n giving an indication of how favorable the adsorption process. The magnitude of the exponent, 1/n, gives an indication of the favorability of adsorption. Values of n > 1 represent favorable adsorption condition.

To determine the constants K_f and n, the linear form of the equation may be used to produce a graph of ln(q_e) against ln(C_e).

$$lnq_e = lnK_f + \left(\frac{1}{n}\right) \ln C_e \tag{4.8}$$

Values of $K_f$and n are calculated from the intercept and slope of the plot respectively.If n = 1 then the partition between the two phases are independent of the concentration. If value of 1/n is below one it indicates a normal adsorption. On the other hand, 1/n being above one indicates cooperative adsorption (Freundlich*et al.*, 1906). K_f and n are parameters characteristic of the sorbent-sorbate system, which must be determined by data fitting and whereas linear regression is generally used to determine the parameters of kinetic and isotherm models.

From Figure 26 (a) the value of 1/n = 0.483 while n=2.07 indicating that the sorption of Cr(VI) unto the magnetic sorbent is favorable and the R^2 value is 0.987.

Figure 26 (b) the value of 1/n = 0.294 while n=3.40 indicating that the sorption of Hg(II) unto the magnetic sorbent is favorable and the R^2 value is 0.977.

Figure 26 shows Freundlich isotherm for Cr(VI) and (b) for Hg (II) ion adsorption from aqueous solution using synthesized Fe_3O_4 NPs adsorbent.

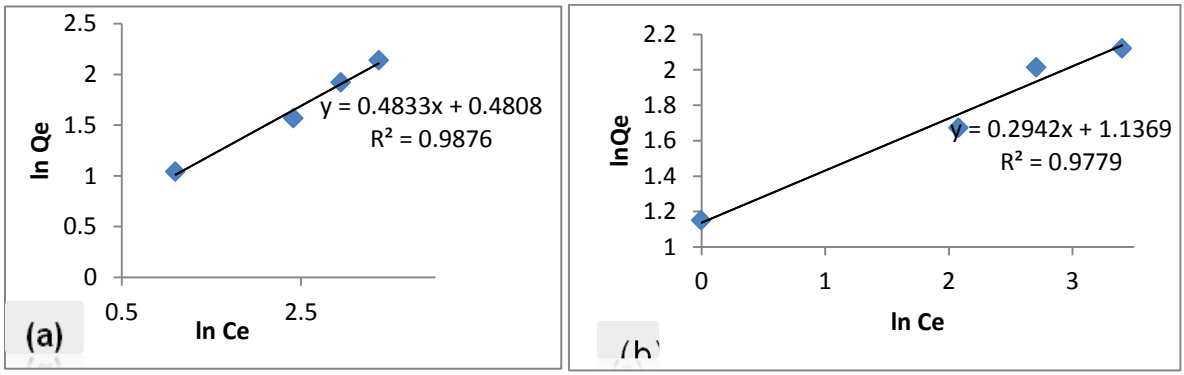

Figure 26: (a) Freundlich isotherm for Cr (VI) and (b) for Hg (II) ion adsorption using synthesized Fe_3O_4 NPs.

Table 9: Langmuir and Freundlich isotherm model constants and correlation coefficients for adsorption of chromium and mercury

Isotherms	Cr(VI)		Hg(II)	
	R^2	Estimated isotherm parameters	R^2	Estimated isotherm parameter
Langmuir	0.93	Q_o(mg/g) = 0.951 K_L(L/mg)= 0.078	0.98	Q_o(mg/g) =2.631 K_L(L/mg)= 0.287
Ferundlich	0.987	K_f=1.614 n =2.07	0.977	K_f =3.16 n =3.40

5. CONCLUSION AND RECOMMENDATIONS

5.1 Conclusion

Fe_3O_4 NPs were synthesized using leaf extract of *Thymus schimperi* and its efficiency for chromium hexavalent, Cr(VI) and mercury divalent, Hg(II) from aqueous solution was examined. Fe_3O_4 NPs was synthesized by the biological synthesis method using aqueous leaf extracts and characterized by advanced techniques.

The XRD study confirms the formation of cubic face centered structure and the crystallite size (20-30 nm) of the synthesized Fe_3O_4 NPs while the vibrational stretching around 573 cm^{-1} Fe_3O_4 NPs were also supports the formation of Fe_3O_4 nanoparticles.

The SEM image analyses revealed that the ratio of iron salts precursors, leaf extract and the grain size of synthesized Fe_3O_4 NPs. The EDS studies confirmed the composition of the synthesized nanoparticles were iron, oxygen in higher and other elements in lower amount.

Of synthesized Fe_3O_4 NPs; S21, S11 and S12 were not sensitive to adsorb metal ions in the same adsorption capacities. S11 showed significant adsorption of Cr(VI) and Hg(II) from aqueous solution.

The percentage removals were found to be dependent on the quantity of sorbent dosages, pH, time, and initial concentration of the two sorbates (chromium and mercury). Pseudo-second-order kinetics model was found to be the predominant for both Cr(VI) and Hg(II). The equilibrium sorption data fitted the Langmuir isotherms with high correlation coefficients, suggesting that the process followed a monolayer adsorption onto a surface containing a finite number of adsorption sites for Cr(VI) and Hg(II). From the result biogenic synthesis of is a better choice due to eco-friendliness.

5.2 Recommendations

- More research is needed to prepare extracts on the other parts of *Thymus schimperi* like flower, root, stem, seed and etc.
- The effect of temperature regarding removal of Hg(II) and Cr(VI) ions using Fe_3O_4 NPs as adsorbent also needs further study.
- Moreover, more experiments should be done with other heavy and toxic metal removal efficiency.
- Regeneration and characterization of Fe_3O_4 NPs after adsorption needs further study.
- Reuse of molten liquids.

6. REFERENCE

Abbasi, E., Aval, S. F., Akbarzadeh, A., Milani, M., Nasrabadi, H.T., Hanifepour, Y., (**2014**). Dendrimers synthesis, applications, and properties.*Nanoscale. Res. Lett*, 9, 247-267.

Adegoke, H.I., (**2013**).Adsorption of Cr(VI) on synthetic hematite (α-Fe_2O_3) nanoparticles of different morphologies. *Korea. J. Chem. Enginee*, 31, 142-154.

Aerosp, J., (**2015**).Nanoparticles and application. *Technol. Manag*, 7, 267-276.

Ai, Z., Deng, K., Wan, Q., Zhang, L., Lee, S., (**2010**). Facile microwave-assisted synthesis and magnetic and gas sensing properties of Fe_3O_4nanoroses. *J. Phys. Chem*,114, 6237.

Akbarzadeh, A., Samiei, M., Davaran, S., (**2012**). Magnetic nanoparticles preparation, physical properties, and applications in biomedicine. *Nanoscale. Res. Lett*, 7, 144-156.

Ansari, R., Fahim, N.K., (**2007**). Application of polypyrrole coated on wood sawdust for removal of Cr(VI) ion from aqueous solutions. *React. Funct.Polym*, 67, 367-374.

Ashokkumar, M., Lee, J., Kentish, S., Grieser, F., (**2007**). Bubbles in an acoustic field. *An overview. Ultrason. Sonochem*, 14, 470-475.

Awwad, A.M., Salem, N.M., (**2012**). Green and facile approach for synthesis of magnetite nanoparticles. *J. Nanosci. Nanotechnol*, 2, 208-213.

Bang, J.H., Suslick, K.S., (**2007**). Sonochemical synthesis of nanosized hollow hematite.*J. Am. Chem. Soc*, 129, 2242-2243.

Basavegowda, N., Magar, K.B.S., Mishra, K., Lee, Y.R., (**2014**). Green fabrication of ferromagnetic Fe_3O_4 nanoparticles and their novel catalytic applications for the synthesis of biologically interesting benzoxazinone and benzthioxazinone derivatives. *J. Chem*, 38, 5415-5420.

Bharde, A.A., Parikh, R.Y., Baidakova, M., Jouen, S., Hannoyer, B., Enoki, T., (**2008**). Bacteria-mediated precursor-dependent biosynthesis of superparamagnetic iron oxide and iron sulfi de nanoparticles. *Langmuir*, 24, 5787-5794.

Bomati-Miguel, O., Mazeina, L., Navrotsky, A., Veintemillas-Verdaguer, S., (**2008**).Calorimetric study of maghemite nanoparticles synthesized by laser-induced pyrolysis.*Chem Mater*, 20, 591-598.

Boxall, C., Kelsall, G and Zhang, Z., **(1996**).Photoelectrophoresis of colloidal iron oxides, Part 2-magnetite (Fe_3O_4).*J. Chem. Soc*, 92, 791-890.

Cabrera, L., Gutierrez, S., Menendez, N., Morales, M.P., Herrasti, P., (**2008**). Magnetite nanoparticles electrochemical synthesis and characterization.*Electrochem.Acta*, 53, 3436-3441.

Cai, W., Wan, J., (**2007**). Facile synthesis of superparamagnetic magnetite nanoparticles in liquid polyols. *J. Colloid. Interf.Sci*, 3, 305-366.

Camara, F.B.G., Costa, L.A., Fidelis, G.P., Nobre, L.T.D.B., Dantas-Santos, N., Cordeiro, S.L., Costa, M.S.S.P., Alves, L.G., Rocha, H.A.O., (**2011**).Heterofucans from the brown seaweed Canistrocarpuscervicornis with anticoagulant and antioxidant activities.*Mater. Drugs*, 9, 124-138.

Cao, M., Li, Z., Wang, J., Ge, W., Yue, T., L. R., Colvin, V. L and Yu,W W., **(2012**). Food related applications of magnetic iron oxide nanoparticles: enzyme immobilization, protein purification, and food analysis. *Food Sci. Technol,* 2, 7-47.

Caruntu, D., Caruntu. G., O'Connor, C. J., (**2007**). Magnetic properties of variable-sized Fe_3O_4 nanoparticles synthesized from non-aqueous homogeneous solutions of polyols. *J. Appl. Phys*, 40, 5780-5801.

Chaki, S.H., Malek, T.J., Chaudhary, M.D, Tailor, J.P., Deshpande,M.P., (**2015**). Magnetite Fe_3O_4 nanoparticles synthesis by wet chemical reduction and their characterization.*Adv. Nat. Sci*, *Nanosci. Nanotechnol*, 6, 1-7.

Chandran, S. P., Chaudhary, M., Pasricha, R., Ahmad, A., Sastry, M., (**2006**).Synthesis of gold nanotriangles and silver nanoparticles using Aloevera plant extract.*Biotechnol.Progr*, 22, 577-583.

Chen, Z., Wang, T., Jin, X., Megharaj, M., Naidu, R., (**2013**). Multifunctional kaolinitesupported nanoscale zerovalent iron used for the adsorption and degradation of crystal violet in aqueous solution. *J. Colloid. Interface. Sci*, 3, 59-66.

Cheng, X.L., Jiang, J.S., Hu, M., Mao, G.Y., Liu, Z.W., Zeng,Y., Zhang, Q.H. (**2012**). Liquid-liquid interfaceassistedsolvothermal synthesis of durian-like α-Fe_2O_3 hollow spheres constructed by nanopolyhedrons.*Crystengcomm*, 14, 3045-3056.

Chin, A.B., Yaacob II., (**2007**). Synthesis and characterization of magnetic iron oxide nanoparticles via water oil microemulsion.*J. Mater. Process.Technol*, 191, 235-237.

Cornell, R.M., Schwertmann, U., (**2003).**The iron oxides, structures, properties, reactions, occurrences and uses.*Lec.Univers.Preserve,* 15, 1-50.

Crist, R.H., Martin, J.R., Chonko, J., (**1996**). Uptake of heavy metals on peat moss: an ion-exchange process.*Environ. Sci. Technol*, 30, 2456-2461.

Dave, P.N and Chopda, L.V., (**2014**).Application of iron oxide nanomaterials for the removal of heavy metals.*J. Nano.Technol*, 9, 1-14.

Demsew, S., (**1993**).The Genus *Thymus (Labiatae)* in Ethiopia, opera.*Biot*, 21, 57-60.

Denizli, A.S., Senel, Alsancak, G., Tu¨zmen, N., Say, R., (**2003**). Mercury removal from synthetic solutions using poly(2-hydroxyethylmethacrylate) gel beads modified with poly(ethyleneimine). *React. Funct.Polym*, 55, 121-130.

Dong, W.T., Zhu, C.S.,(**2002**).Use of ethylene oxide in the sol-gel synthesis of α-Fe2O3 nanoparticles from Fe(III) salts. *J. Mater. Chem*, 12, 16-76.

Eatemadi, A., Daraee, H., Zarghami, N., Yar, H.M., Akbarzadeh, A., Hanifehpour, Y., (**2014**). Nanofiber synthesis and biomedical applications.*Artif.Cell.Nanomed.Biotechnol*, 1-11.

Faraji, M., Yamini, Y., Rezaee, M., (**2010**).Magnetic nanoparticles: synthesis, stabilization, functionalization, characterization and applications. *J. Iran. Chem. Soc*, 7, 1-37.

Fengshi, C., Shixin, Z., Zhihao, Y., (**2015**).Effect of γ-Fe_2O_3 nanoparticles on the efficiency of dye-sensitized solar cells.*Resear. Adv.* 5, 1-6.

Feynman, R., (**1991**).There's plenty of room at the bottom.*Science*,254, 1300-1301.

Forough, M., Fahadi, K., (**2011**).Biological and green synthesis of silver nanoparticles.*Turkish. J. Eng. Environ. Sci*, 34, 281-287.

Freundlich, H.M.F.,(**1906**). Over the adsorption in solution.*Z. Phys. Chem*, 57, 385-470.

Gangadhara, G., Maheshwarib, U., and Gupta, S., (**2012**).Nanoparticles synthesis and application.*Nano. Sci. Technol*, 2, 140-150.

Ghandoor,H.El.,Zidan, H.M., Mostafa, M.H.K., Ismail, M.I.M.,(**2012**).Synthesis and some physical properties of magnetite (Fe_3O_4) nanoparticles.*Int. J. Electrochem. Sci*,7, 1-12.

Gotic, M., Jurkin, T., Music, S., (**2009**). Iron (III) precursor to magnetite and vice versa. *Mater.Resear. Bulletin*, 44, 2014-2021.

Gui, M., Smuleac, V., Ormsbee, L.E., Sedlak, D.L., Bhattacharyya, D., (**2012**). Iron oxide nanoparticle synthesis in aqueous and membrane systems for oxidative degradation of trichloroethylene from water. *J.Nanoparticles. Resear.* 14, 1-16.

Guo, L., Huang, Q., Li, X., Yang, S., (**2001**). Iron oxide nanoparticles synthesis and applications in surface enhanced raman scattering and electrocatalysis. *Phys. Chem*, 3, 1661-1665.

Gupta, R.K., Singh, R.A., Dubey, S.S., (**2004**). Removal of mercury ions from aqueous solutions by composite of polyaniline with polystyrene.*Sep.Purif. Technol*, 38, 225-232.

Herlekar, M., Barve,S., (**2015**).Calcination and microwave assisted biological synthesis of iron oxide nanoparticles.*Int. Res. J. Env.Sci*, 4, 28-36.

Hu, L., Percheron, A., Chaumont, D., Brachais, C.H., (**2011**). Microwave-assisted one-step hydrothermal synthesis of pure iron oxide nanoparticles (magnetite, maghemite and hematite). *J. Sol-Gel. Sci. Technol*, 60, 1-98.

Hua, M.,(**2012**).Heavy metal removal from water/wastewater by nanosized metal oxides.*Review. J. Hazard Mater*, 212, 317-331.

Indira, T. K., Lakshmi, P. K., (**2010**). Magnetic nanoparticles.*Int. J. Pharm. Sci. Nanotechnol*, 3, 1035-1042.

Iravani, S., (**2011**).Green synthesis of metal nanoparticles using plants. *Green Chem*, 13, 2638-2650.

Ji, G., Lin, X., Liu, Y., Huang, Q., Yang, Z., du, Y., (**2012**).Formation mechanism and magnetic properties of hollow Fe_3O_4nano-spheres synthsized without any surfactant *Crystengcomm*,14, 8658-8680.

Jiang, C.,Wu, W.Z W.,Yu, T., Kim, W.S., (**2015**).Recent progress on magnetic iron oxide Nanoparticles. *Sci. Technol. Adv. Mater*. 16, 1-43.

Johari, K., Saman, N., Tien, S.S., Chin, C.S., Kong, H., Mat, H., (**2016**). Removal of elemental mercury and chromium by coconut pith char adsorbents. *Procedia*, 148, 1357-1362.

Kanaga, S. S., Kadirvelu, K., (**2017**). Green synthesis of iron oxide nanoparticles. *Sci.J.* 2, 422-427.

Kang, X., Jia, C.Y., Wan, Z.Q., Zhuang, J., Feng, J., (**2015**).Solar cell application. *J. Resea.Adv*, 5, 16678-16683.

Kumar, B., Smita, K., Cumbal, L., Debut, A., (**2014**).Biogenic synthesis of iron oxide nanoparticles for arylbenzimidazole fabrication. *J. Saudi. Chem. Soc*, 18, 364-369.

Langmuir, I., (**1916**). The constitution and fundamental properties of solids and liquids.*J.Americ.Chem. So*, 38,2221-2295.

Langmuir, I.,(**1918**). The adsorption of gases on plane surfaces of glass, mica and platinum.*J.Am. Chem. Soc*, 40, 1361-1403.

Laudise, R. A., (**2004**). Hydrothermal synthesis of crystals. *A Reprint Collection (Amsterdam: Elsevier)*, 185- 202.

Laurent, S., Forge, D., Port, M., Roch, A., Robic, C., Vander Elst, L and Muller., R.N., (**2008**). Magnetic iron oxide nanoparticles: Synthesis, stabilization, physicochemical characterizations and biological applications. *Chem. Review*, 108, 2064-2110.

Lin, K. S., Chang, N. B., Chuang, T. D., (**2008**). Fine structure characterization of zerovalent iron nanoparticles for decontamination of nitrites and nitrates in wastewater and groundwater.*Sci. Technol. Adv.* Mater, 9, 1-5.

Lu, A.H., Salabas, E.L and Schuth, F., (2**007**).Magnetic nanoparticles: synthesis, protection, functionalization, and application.*Chem. Int. Educ*, 46, 12-22.

Machala, L., Tucek, J., Zboril, R., (**2011**).Polymorphous transformations of nanometric iron (III) oxide. *Chem, review.* Mater, 23, 3255-3272.

Madhu, G.C., Pavithra, V., Jaianand, K., Balaji, P., (**2017**). Green synthesis and characterization of iron oxide nanoparticles. *Int. J. Agricult. Innov. Res*, 6, 1-9.

Mahdavi, M., Namvar, F., Ahmad, M. B., Mohamad, R., (**2013**).Green biosynthesis and characterization of magnetic iron oxide (Fe_3O_4) nanoparticles using seaweed (Sargassummuticum) aqueous extract.*Scie. J. Molecu*, 18, 5954-5969.

Mihir.H., Siddhivinayak, B., Rakesh. K.,(**2014**). Plant-mediated green synthesis of iron nanoparticles, 89, 1-10 (http://dx.doi.org/10.1155/2014/140614).

Mittal, K., Chisti, Y., Banerjee, U.C., (**2013**).Green synthesis using various plant extract.*Bio. Technol. Adv*, 31, 346-356.

Mohan, D., Pittman C.U. J., (**2006**).Activated carbons and low cost adsorbents for remediation of tri- and hexavalent chromium from water. *J. Hazard. Mater*, 137, 762-811.

MohanKumar, K., Mandal, B.K., Siva Kumar., K, Sreedhara, R.P,, Sreedhar, B., (**2013**).Bio-based green method to synthesize palladium and iron nanoparticles using Terminaliachebula aqueous extract. *Spectro.Chem. Acta.* A, 102, 128-133.

Mohd, A., Sumbul, R., Masood, Alam., Arulazhagan, P., (**2013**).Adsorption of Hg(II) from aqueous solution using Adulsa (Justiciaadhatoda) leaves powder. *J. Chem*, 11, 1-12.

Moulik, S. P., Paul, B. K., (**1998**). Structure, dynamics and transport properties of microemulsions. *Adv. Colloid. Interf.Sci*, 78, 99-195.

Murray, C.B., Kagan, C.R., Bawendi, M.G., (**2000**).Synthesis and characterization of monodispersenanocrystals and close-packed nanocrystalassemblies, *Annual.review.Mater. J. Sci*,30, 545-610.

Naik, R.R., Stringer, S.J., Agarwal, G., Jones, S., Stone, M.O., (**2002**).Biomimetic synthesis and patterning of silver nanoparticles.*Natural. Mater*, 1, 169-172.

Nigist, A., Storesund, H. J., Skattebol, L., Tonnesen, F., Aasen, A.J., (**2000**).*Volatile oil constituents of two Thymus species from Ethiopia. Int.J.Sci.*15,123-125.

Osborne, E.A., Atkins, T M., Gilbert, D.A., Kauzlarich, S.M., Liu, K., Louie, A.Y., (**2012**).Rapid microwave-assisted synthesis of dextran-coated iron oxide nanoparticles for magnetic resonance imaging.*Nanotechnol*, 23, 215-602.

Padil, V.V., Cerník, M., (**2013**).Green synthesis of copper oxide nanoparticles using gum karaya as biotemplate and their antibacterial application.*Int. J. Nanomedicine*, 8, 889-898.

Padmavathy, K.S., Madhu, G., Haseena. P.V.,(**2016**).Effects of pH, adsorbent dosage, time, initial concentration and adsorption isotherm study for the removal of hexavalent chromium (Cr (VI)) from wastewater by magnetite nanoparticles. *Int. Conf. Eng. Sci. Techno*, 24, 585-594.

Pandey, S., Mishra, S., (**2011**).Sol-gel derived organic-inorganic hybrid materials: synthesis, characterizations andapplications. *J. Sol-Gel. Sci. Technol*, 5, 59-73.

Pandey, S., Oza, G., Mewada, A., Sharon, M., (**2012**).Green synthesis of highly stable gold nanoparticles using Momordicacharantia as nano fabricator.*Appl. Sci. Res*, 4, 1135-1141.

Panigrahi, S.,Kundu, S., Ghosh, S. K., Nath, S., Pal, T., (**2004**). General method of synthesis for metal nanoparticles.*J. Nanoparticles.Resear*, 6, 411-414.

Pascu, O., Carenza, E., Gich, M., Estrade, S., Peiro, F., Herranz, G., Roig, A., (**2012**). Surface reactivity of iron oxide nanoparticles by microwave-assisted synthesis; comparison with the thermal decomposition route. *J. Phys. Chem*,116, 15-108.

Patra, J.K., Ali, M.S., Oh, I.G., Baek, K.H., (**2017**).Proteasome inhibitory, antioxidant, and synergistic antibacterial and anticandidal activity of green biosynthesized magnetic Fe_3O_4 nanoparticles using the aqueous extract of corn (Zea mays L.) ear leaves.*Artif.Cells Nanomed.Biotechnol*, 45, 349-356.

Paull, R., Wolfe, J., Hebert P., Sinkula, M., (**2003**).Investing in nanotechnology.*Natural.Bio. Techno*,21, 1134-1147.

Petla, K., Vivekanandhan, S., Misra, M., Mohanty, A.K., Satyanarayana, N., (**2012**). 'soybean (glycine max) leaf extract based green synthesis of palladium nanoparticles. *J. Biomat. Nanobiotechnol,* 3, 14-19.

Pourhassan-Moghaddam, M., Zarghami, N., Mohsenifar, A., Rahmati- Yamchi, M., Gholizadeh, D., Akbarzadeh, A., (**2014**).Water cress based gold nanoparticles biosynthesis, mechanism of formation and study of their biocompatibility in vitro. *J, Nano*, 4, 5-12.

Prasad, A.S., (**2016**).Iron oxide nanoparticles synthesized by bioprecipitation using leaf extract of garlic vine (Mansoaalliacea).*Mater. Sci. Semicond. Process*, 53, 79-83.

Qin, Li., Sun, Li., Zhang, Y., Qian, Y., Zhai, J., (2**011**). Characteristics of equilibrium, kinetics studies for adsorption of Hg(II) and Cr(VI) by polyaniline/humic acid composite. *J.* 266, 188-194.

Qiu, G., Huang, H., Genuino, H., Opembe, N., Stafford, L., Dharmarathna, S., Suib, S. L., (**2011**).Microwave-assisted hydrothermal synthesis of nanosized α-Fe2O3 for catalysts and adsorbents.*J. Phys. Chem*, 115, 196-265.

Raveendran, P., Jie, F., Scott. L. W., (**2003**). Completely green synthesis and stabilization of metal nanoparticles.*J. Am. Chem. Soc.*125, 13940-13941.

Saif, S., Tahir, A.Y., Chen., (**2016**).Nanoparticles synthesis.*Nano.Mater*, 6, 209-212.

Salam,H.A., Rajiv, P., Kamaraj, M., Jagadeeswaran, P., Gunalan, S., Sivaraj, R., (**2012**).Plants green route for nanoparticle synthesis. *Int. Res. J. Biol. Sci*, 1, 85-90.

Sanpo, N., Berndt, C.C., Wen, C., Wang, J., (**2013**). Transition metal-substituted cobalt ferrite nanoparticles forbiomedical applications.*Acta, biomaterial*, 9, 5830-5837.

Santos, S.A.O., Villaverde, J.J, Freire, C.S.R., Domingues, M.R.M., Neto, C.P., Silvestre, A.J.D., (**2012**). Phenolic composition and antioxidant activity of *Eucalyptus grandis, E. urograndis and E.maidenii* bark extracts. *Ind. Crop. Prod*, 39, 120-127.

Scheffel, A., Gruska, M., Faivre, D., Linaroudis, A., Plitzko, M., Schuler, D., (**2006**). An acidic protein aligns magnetosomes along a filamentous structure in magneto tactic bacteria. *Nature,* 4, 40-110.

Senthil, M., Ramesh, C., (**2012**). Biogenic synthesis of Fe_3O_4 nanoparticles using Tridaxprocumbens leaf extract and its antibacterial activity on Pseudomonas aeruginosa. *J. Nano. Mater. Bio. Structure,* 7, 1655-1660.

Shen, Y.F., Tang, J., Nie, Z.H., Wang, Y.D., Ren, Y., Zuo, L., (**2009**). Preparation and application of magnetic Fe_3O_4 nanoparticles for wastewater purification. *Sep. Purif. Technol*, 68, 3-12.

Smith, B., (**1998**). Infrared spectral interpretation.*System. Appro.3*, 4-78.

Song, J.Y., Kim, B.S., (**2009**). Rapid biological synthesis of silver nanoparticles using plant leaf extracts. *Bioprocess. Biosyst. Eng*, 32, 79-84.

Sravanthi, M., Muni Kumar, D., Ravichandra, M., Vasu,G., Hemalatha, K.P.J., (**2016**). Green synthesis and characterization of iron oxide nanoparticles using WrightiatinctoriaLeaf Extract. *Int. J .Curr. Resear. Aca. Rev*, 4, 30-44.

Sun, J.,Zhou,S., Hou, P., Yang, Y., Weng, J., Li, X., (**2007**). Synthesis and characterization of biocompatible Fe_3O_4nanoparticles. *J. Biomed. Mater. Resear*, 80, 333-341.

Tartaj, P., del Puerto Morales, M., Veintemillas-Verdaguer, S., González-Carreño, T., Serna, C. J., (**2003**). The preparation of magnetic nanoparticles for applications in biomedicine. *J. Appl. Phys*, 6, 36-182.

Thakkar,K.N., Mhatre, S.S., Parikh, R.Y., (**2010**). Biological synthesis of metallic nanoparticles. *Nanomedicine*, 6, 257-262.

Venkateswarlu, S., Natesh Kumar, B., Prasad, H., Venkateswarlu, P., Jyothi, V., (**2014**). Bioinspired green synthesis of Fe_3O_4 spherical magnetic nanoparticles using Syzygiumcumini seed extract. *Physic. Bio.Technol*, 4, 67-71.

Venkateswarlu, S., Rao, S., Balaji, T., Prathima, BandJyothi, N.V., (**2013**). Biogenic synthesis of Fe_3O_4 magnetic nanoparticles using plantain peel extract. *Matter. Letter*, 100, 241-244.

Vicky, M., Rodney, S., Ajay, S., Hardik, M., (**2010**). Introduction to metallic nanoparticles.*J. Pharm. Bio appli.Sci*, 2, 282-289.

Vigneshwaran, N., Ashtaputre, N.M., Varadarajan, P.V., Nachane, R.P., Paralikar, K.M., Balasubramanya, R.H., (**2007**). Biological synthesis of silver nanoparticles using the fungus Aspergillusflavus. *Mater. Lett*, 61, 1413-1418.

Walton, R. I., (**2002**). Subcritical solvothermal synthesis of condensed inorganic materials. *Chem. Soc. Rev*, 31, 2-30.

Wan Ngah, W.S., Hanafiah, M. A. K. M., (**2008**). Removal of heavy metal ions from wastewater by chemically modified plant wastes as adsorbents. *Review, Bio. Technol*, 99, 3935-3948.

Willard, M.A, Kurihara, L.K, Carpenter, E.E., Calvin, S., Harris, V.G., (**2004**). Chemically prepared magnetic nanoparticles. *Int. Mater. Rev*, 49, 125-170.

Willner, I., Baron, R., Willner, B., (**2006**). Growing metal nanoparticles by enzymes.*Adv. Mater*, 18, 1109-1120.

Woo, K., Hong, J., Choi, S., Lee, H.W., Ahn, J.P., Kim, C.S., Lee, S.W., (**2004**). Easy synthesis and magnetic properties of iron oxide nanoparticles.*Chem. Mater*, 16, 2814-2818.

Wu, L.H., Yao, H.B., Hu, B., Yu, S.H., (**2011**). Unique lamellar sodium/potassium iron oxide nanosheets: Facile microwaveassisted synthesis and magnetic and electrochemical properties. *Chem. Mater*, 23, 39-46.

Wu, W., He, Q., Jiang, C., (**2008**). Magnetic iron oxide nanoparticles, synthesis and surface functionalization strategies.*Nanoscale. Res. Lett*, 3, 397-415.

Wu, W., Xiao, X.H., Zhang, S.F., Zhou, J.A., Fan, L.X., Ren, F., Jiang, C, Z., (**2010**). Large-scale and controlled synthesis of iron oxide magnetic short nanotubes: shape evolution, growth mechanism, and magnetic properties. *J. Phys. Chem,* 114, 16-92.

Xiao, X.H., Zhang, S.F., Peng, T.C., Zhou, J., Ren, F., Jiang, C.Z., (**2010**). Synthesis and magnetic properties of maghemite (γ-Fe_2O_3) short-nanotubes. Nanosc. *Resear. Lette*, 5, 17-74.

Ya, P., Guangming, Z., Lin, T., Yi, Z., Yuanyuan, L., Xiaoxia, L., Zhen, L., Jiachao, Z, Zhifeng, L., Yiqun, X., (**2011**). Preparation and application of stability enhanced magnetic nanoparticles for rapid removal of Cr(VI)and Hg(II). *Chem. Eng. J*, 175, 222-227.

Yamaura, M., Camilo, R.L., Sampaio, L.C., Macedo, M.A., Nakamura, M., Toma, H.E., **(2004**). Preparation and characterization of (3-aminopropyl) triethoxysilane-coated magnetite nanoparticles.*J. Mater*, 2, 79-210.

Yew, Y.P., Shameli, K., Mikio, M., Khairudin, N.A., Mohamad., S.B., Takeru, N.,Kar, X.L., (**2018**). Green biosynthesis of superparamagnetic magnetite Fe_3O_4 nanoparticles and biomedical applications in targeted anticancer drug delivery system. *J. Chem*, 4, 1-22.

APPENDICES

Appendix 1: XRD pattern for S21

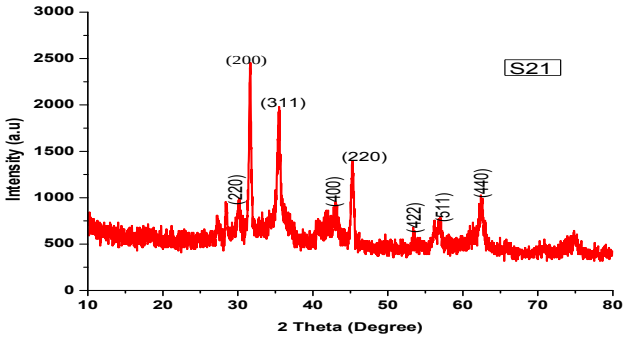

Appendix 2: XRD pattern for S12

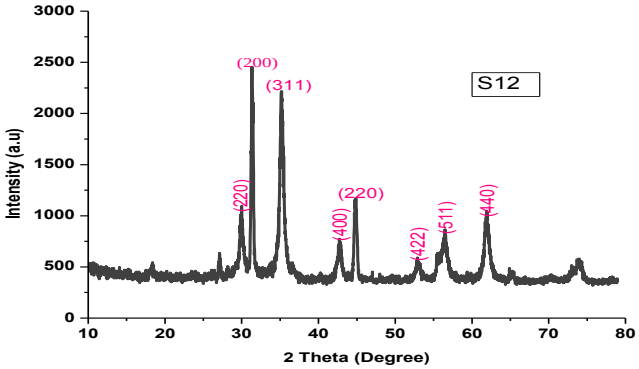

Appendix 3: Standard solution curve for Cr(VI) solution

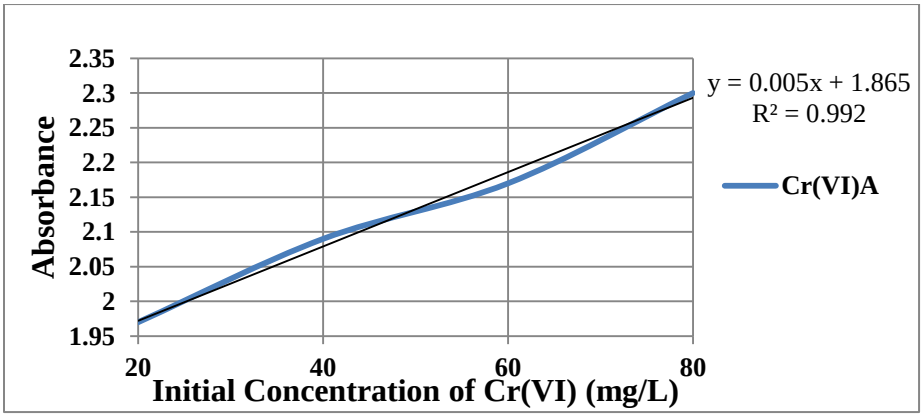

Appendix 4: Standard solution curve for Hg(II) solution

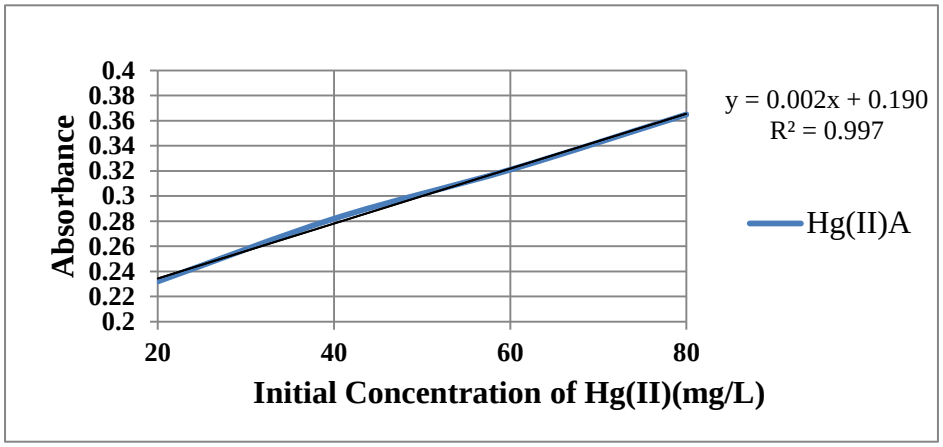

Appendix 5: Optimum results of different parameters

Parameters	Optimization result seen	
	Cr (VI)	Hg(II)
Concentration	20	20
PH	5	7
Adsorbent dosage	700	700
Contact time	90	90

Appendix 6: Powders of S12, S11 and S21 from left to right respectively.